1146 J. Med. Chem. 2010, 53, 1146–1158
DOI: 10.1021/jm901414e

Journal of Medicinal Chemistry Article

Design and Synthesis of 5,5′-Disubstituted Aminohydantoins as Potent and Selective Human β-Secretase (BACE1) Inhibitors

Michael S. Malamas,*,† Jim Erdei,† Iwan Gunawan,† Jim Turner,‡ Yun Hu,‡ Erik Wagner,‡ Kristi Fan,† Rajiv Chopra,§ Andrea Olland,§ Jonathan Bard,‡ Steve Jacobsen,‡ Ronald L. Magolda,† Menelas Pangalos,‡ and Albert J. Robichaud†

†Department of Chemical Sciences, Wyeth Research, CN 8000, Princeton, New Jersey 08543-8000, ‡Neuroscience, Wyeth Research, CN 8000, Princeton, New Jersey 08543-8000, and §Department of Chemical Sciences, Wyeth Research, 200 Cambridge Park Drive, Cambridge, Massachusetts 02140

Received September 22, 2009

The identification of small molecule aminohydantoins as potent and selective human β-secretase inhibitors is reported. These analogues exhibit low nannomolar potency for BACE1, show comparable activity in a cell-based (ELISA) assay, and demonstrate >100× selectivity for the other structurally related aspartyl proteases BACE2, cathepsinD, renin, and pepsin. On the basis of the cocrystal structure of the HTS-hit **2** in the BACE1 active site and by use of a structure-based drug design approach, we methodically explored the comparatively large binding pocket of the BACE1 enzyme and identified key interactions between the ligand and the protein that contributed to the affinity. One of the more potent compounds, (*S*)-**55**, displayed an IC_{50} value for BACE1 of 10 nM and exhibited comparable cellular activity (EC_{50} = 20 nM) in the ELISA assay. Acute oral administration of (*S*)-**55** at 100 mg/kg resulted in a 69% reduction of plasma $A\beta_{40}$ at 8 h in a Tg2576 mouse ($p < 0.001$).

Introduction

Alzheimer's disease (AD[a]) is a progressive, degenerative disease of the brain and the leading cause of dementia. At the early stage, AD is associated with gradual loss of cognition that leads to complete deterioration of cognitive and behavioral functions and ultimately death. AD is a debilitating disease that affects millions of elderly men and women worldwide and has been recognized as a major global social and financial burden.[1,2] The prognosis of AD is poor, and there is a great need for medical intervention of this disease. Currently, the approved medical therapies consist of cholinesterase inhibitors and *N*-methyl D-aspartate (NMDA) antagonists that reduce the symptomatology of the disease in the initial phase but are not capable of curing or stopping its progression.[3,4] The pathological hallmarks of AD include the extracellular deposition of β-amyloid peptide (Aβ), which leads to aggregation and plaque formation, and the abnormal hyperphosphorylation of tau protein, which leads to the intracellular formation of neurofibrillary tangles.[5,6] β-Amyloid deposits are predominately aggregates of the Aβ peptides (Aβ, 39−43 residues) resulting from the endoproteolysis of the amyloid precursor protein (APP).[7,8] These peptide fragments result from the sequential cleavage of APP, first at the N-terminus by β-secretase enzyme (β-site APP cleaving enzyme, BACE1),[9−11] followed at the C-terminus by one or more γ-secretase complexes (intramembrane aspartyl proteases),[12] as part of the β-amyloidogenic pathway. More specifically, BACE1 cleaves APP to generate secreted peptide sAPPβ and the membrane bound C99 fragment, which is then cleaved by γ-secretase complexes to produce peptide $A\beta_{40}$ as the predominant product (90% abundance) and peptide $A\beta_{42}$ as a minor product (9% abundance). Peptide $A\beta_{42}$ is reportedly the more highly pathogenic and the primary source of plaque formation. Although the cause of AD remains unknown, a large body of evidence is beginning to accumulate that highlights the central role of Aβ in the pathogenesis of the disease.[13−17] Thus, processes that limit Aβ production and deposition by preventing formation, inhibiting aggregation, and/or enhancing clearance may offer effective treatments for AD. Since β-secretase mediated cleavage of APP is the first and rate-limiting step of the amyloidogenic processing pathway, BACE1 inhibition is considered a prominent therapeutic target for treating AD by diminishing Aβ peptide formation in AD patients.

Since the identification of a BACE1 knockout mouse and the subsequent characterization of its viability, the interest in this enzyme has been significant among researchers in the AD area. Over the past decade multiple groups have investigated a variety of approaches to the design of BACE1 inhibitors. The initial work by Tang and Ghosh was concentrated on peptidic substrate transition-state mimic inhibitors.[18] These ligands showed excellent low nanomolar inhibitory potency for BACE1 but had limited potential as oral CNS drug candidates because of their poor pharmacokinetic properties. These initial findings, together with a coordinated drug design

*To whom correspondence should be addressed. Telephone: 732-274-4428. Facsimile: 732-274-4505. E-mail: malamam@wyeth.com.

[a] Abbreviations. AD, Alzheimer's disease; Aβ, β-amyloid peptide; APP, β-amyloid precursor protein; BACE, β-site APP cleaving enzyme; FRET, fluorescence resonance energy transfer; NMDA, *N*-methyl D-aspartate; Abz, *o*-aminobenzoic acid; Dpa, 3-(2,4-dinitrophenyl)-L-2,3-diaminopropionic amide; Dnp, 6-(2,4-dinitrophenyl); MOCAc, 7-methoxycoumarin-4-yl; EDANS, 5-[(2-aminoethyl)amino]naphthalene-1-sulfonic acid; DABCYL, 4,4-dimethylaminoazobenzene-4′-carboxylic acid; ELISA, enzyme-linked immune sandwich assay; CHO, Chinese hamster ovary.

 Published on Web 12/07/2009

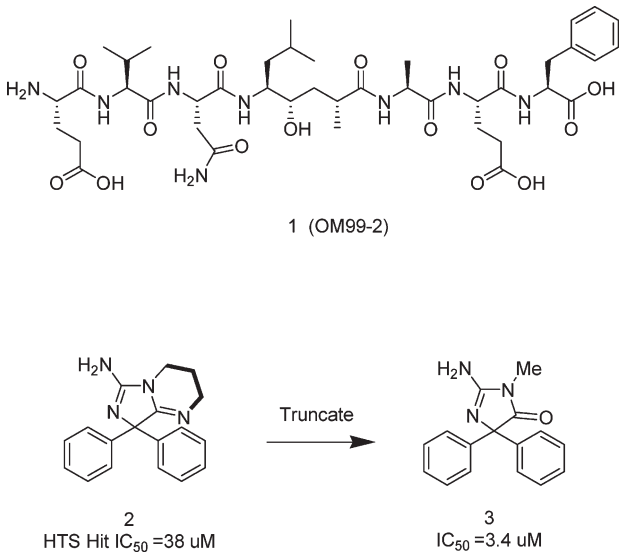

Figure 1

structure-based approach, have paved the way for the generation of less peptidic, second-generation inhibitors.[19−25] The work of Tang (Oklahoma Medical Research Foundation) and Ghosh (University of Illinois at Chicago/Purdue University) has pioneered the evolution of substrate-based inhibitors centered on OM99-2[26] (**1**, Figure 1), a highly potent peptide-derived BACE1 inhibitor (IC_{50} = 1.6 nM). The X-ray crystal of **1** in a complex with BACE1 has sparked the way forward for many new classes of BACE1 inhibitors. These efforts have produced low molecular weight BACE1 inhibitors with little or no peptidic character.[27−32] In addition, recent reports have revealed the application of fragment-based lead generation computational approaches as an alternative path to the design of potent small-molecule BACE1 inhibitors.[33−36] The discovery of low molecular weight BACE1 inhibitors has also led to the improvement of the physicochemical properties of the compounds, as demonstrated by their high-permeability in cell-based assays.[37a−m]

In this paper, we report the design and synthesis of potent and selective BACE1 inhibitors, which originated from the HTS hit **2** (Figure 1). As we have previously reported, lead compound **2** was discovered through a FRET assay screen of our in-house sample collection. It possessed moderate in vitro potency for the BACE1 enzyme with an IC_{50} of 38 μM and demonstrated similar cell-based ELISA potency with an IC_{50} of 27 μM. The crystal structure of **2** in a complex with BACE1 was resolved to 2.3 Å (Figure 2), defining the three-dimensional structure of the enzyme, and revealed that compound **2** occupies the center of the rather large BACE1 binding pocket (S1, S2′ regions) in an orientation where the imidazole ring of the ligand directly interacts with both catalytic-site aspartic acids (Asp32 and Asp228) via a hydrogen-bonding network. Further examination shows that the six-member tetrahydropyrimidine ring points toward solvent space and makes no apparent beneficial contact with residues of the enzyme's backbone. The ensuing truncation of this ring led to the more compact aminohydantoin **3** (Figure 1), which possessed a 10-fold enhancement in potency (IC_{50} = 3.4 μM) as a consequence. The structure−activity relationship studies around compound **3** are the central focus of this report.

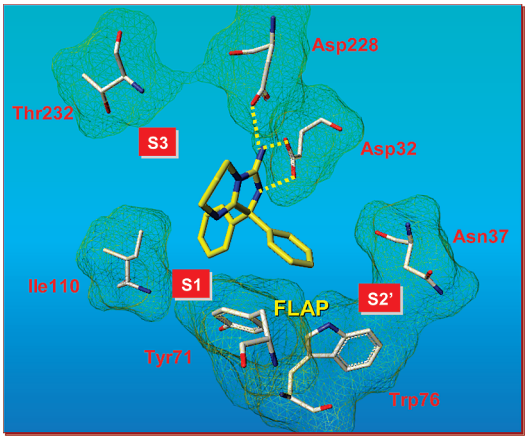

Figure 2. Crystal structure of BACE1 complexed with **2** highlighting the three key hydrogen-bonding interactions between the catalytic aspartic acids Asp32 and Asp228 and the aminoimidazole moiety.

Chemistry

The compounds needed to delineate the SAR for this study were prepared according to Schemes 1−3. An important step for the preparation of the advanced aminohydantoins **10a**,**b** (Scheme 1) was the treatment of 1,2 disubstituted diketones **8a**,**b** with appropriately functionalized 1-alkylguanidines **9** in the presence of base (Na_2CO_3 or K_2CO_3) to produce the desired products in excellent yields. Working in reverse fashion, the required diketones **8a**,**b** for this transformation were either commercially available or prepared straightforwardly via several synthetic routes described in Schemes 1 and 2. In general, two routes were used for the formation of these diketones **8a**,**b**. In route a, commercially available benzyl bromides or chlorides **4** were converted to phosphonium salts **5** upon treatment with triphenylphospine. These phosphonium salts **5** were initially treated with a suitable base (*n*-butyllithium or potassium *tert*-butoxide) and then with the requisite chlorides **6a**,**b** to furnish ylides **7a**,**b**. The required acid chlorides **6a**,**b** were either commercially available or prepared from the corresponding carboxylic acids upon treatment with oxalyl chloride. Oxidation of ylides **7a**,**b** with potassium permanganate in the presence of magnesium sulfate produced diketones **8a**,**b**. Following route b, diethyl oxalate was treated with a suitable Grignard reagent **11** to produce keto esters **12**, which upon hydrolysis to the corresponding carboxylic acids and further treatment with oxalyl chloride afforded glycolic chlorides **13**. A second treatment of chlorides **13** with a diverse Grignard reagent **14** furnished variably functionalized diketones **8a** in excellent yields.

An alternative synthetic approach to the diketones **8a**,**b** is described in Scheme 2, where commercially available benzaldehydes **15** were treated with triethyl phosphite and chlorotrimethylsilane to produce silyl ethers **16**. These were then converted to silyloxy ethers **18a**,**b** upon sequential treatment with lithium diisopropylamide and suitable acid chlorides **17a**,**b**. Hydrolysis of the silyloxy ethers **18a**,**b** with sodium bicarbonate afforded the diketones **8a**,**b**, which were converted to the aminohydantoins **10a**,**b**, as before.

The synthetic approach of Scheme 3 was utilized for the preparation of highly functionalized aminohydantoin derivatives contained in Tables 3−6. Here again, the approach utilizes two alternative strategies to increase the diversity

Scheme 1[a]

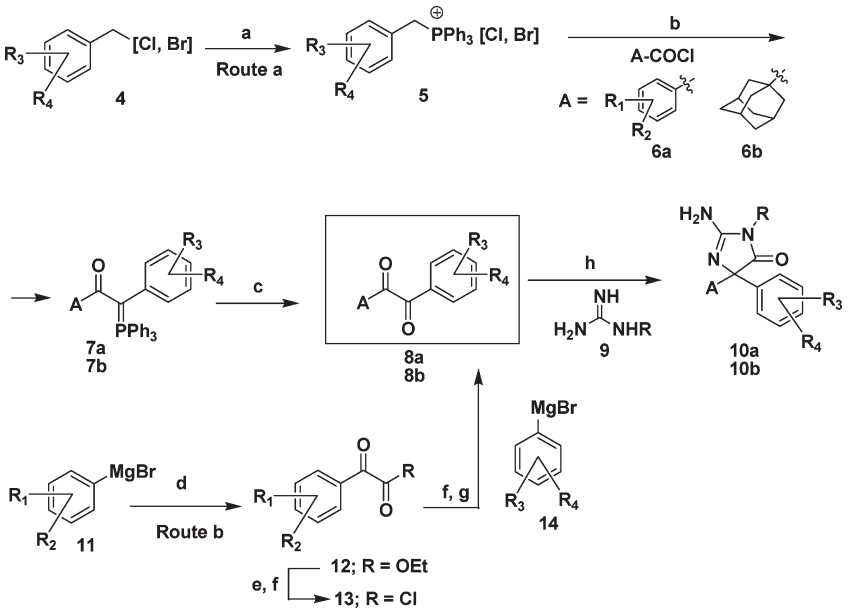

[a] Reagents: (a) PPh_3, toluene; (b) Ar-COCl, *tert*-BuOK, THF; (c) $KMnO_4$, acetone; (d) $(CO_2Et)_2$, THF; (e) aq K_2CO_3, EtOH; (f) $SOCl_2$ or $(COCl)_2$; (g) Ar-MgBr, CuBr, LiBr; (h) $RNH(C{=}NH)NH_2$, K_2CO_3, dioxane, H_2O.

Scheme 2[a]

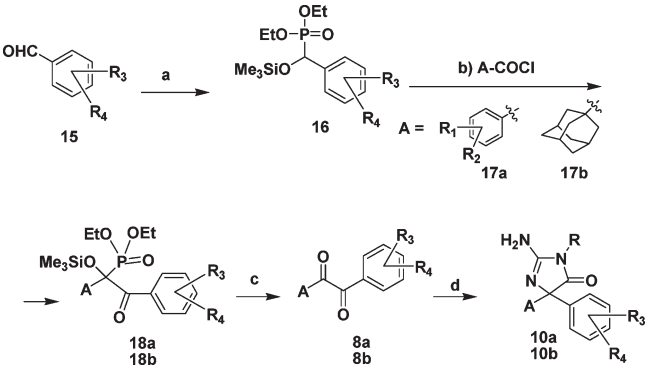

[a] Reagents: (a) $P(OEt)_3$, $ClSiMe_3$, toluene; (b) LDA, THF, A-COCl; (c) $NaHCO_3$, H_2O; (d) $RNH(C{=}NH)NH_2$, Na_2CO_3, EtOH, H_2O.

and efficiency in preparation of multiple analogues in this series. In route a, palladium-catalyzed cross-coupling reaction of key diketones **8a** with any number of heteroarylboronic acids (Suzuki coupling[38]) or heteroaryl trialykl/triaryl stannanes (Stille coupling[39]) in the presence of Pd(0) or Pd(II) catalysts under a variety of well-known conditions produced the desired products **20**. Subsequent condensation of diketones **20** with suitable 1-alkylguanidines **10**, as before, furnished aminohydantoins **21**. In route b, the reverse order of these two reactions is utilized to broaden the scope and breadth of the SAR investigation. In this case, we first converted diketones **8** to aminohydantoins **22** and then utilize the Suzuki or Stille palladium-catalyzed cross-coupling protocols to obtain the desired products **21**.

Results and Discussion

The primary screening assay utilized for the program was a homogeneous, continuous fluorescence resonance energy transfer (FRET) protocol, representing competitive inhibition for BACE1, BACE2, cathepsin D, pepsin, and renin activities.[40] The BACE1 and BACE2 affinities were based on the cleavage of peptide substrate Abz-SEVNLDAEFR-Dpa (Swedish substrate), while peptide substrate MOCAc-GKPILFFRLK (Dnp)-D-R-NH_2 was used for cathepsin D and pepsin, and peptide substrate RE(EDANS)-IHPFHLVIHTK(DABCYL)-R for renin. Kinetic rates were calculated, and IC_{50} values were determined by fitting the % inhibition as a function of compound concentration to the Hill equation ($y = ((B \times Kn) + (100 \times xn))/(Kn + xn)$).

We have routinely screened all prepared compounds for BACE1, BACE2, and cathepsin D inhibition, and only selected compounds were assayed in the pepsin and renin screens, based on their meeting the screening protocol for affinity to the target, and are reported in Tables 1−7.

The cell-based Aβ inhibition (Aβ_{40} or Aβ_{42}) of the potential inhibitors was assessed in an enzyme-linked immune sandwich assay (ELISA) in Chinese hamster ovary (CHO) cells, recombinantly expressing human wild-type APP (CHO-wt). The concentration at which the cellular production of Aβ_{40} or Aβ_{42} was reduced by 50% (EC_{50}) was determined and reported in the tables. Potential compound toxicity was assessed via mitochondrial function using MTS readout (MTS kit from Promega); values are represented as LD_{50} or the dose of compound that resulted in 50% of control signal. MTS data will be discussed only for compounds indicating toxicity concerns.

As previously described,[41] high-throughput screening hit imidazole **2** (Figure 1) was successfully cocrystallized with BACE1 enzyme to 2.3 Å resolution (Figure 2). There are several notable features of the ligand binding interactions. First, the X-ray structure shows that the amino group of the ligand interacts with both aspartic acids (Asp32 and Asp228) and the N3 nitrogen of the imidazole ring interacts with Asp32 via a hydrogen-bonding network. Furthermore, the BACE1/**2** structure indicates that the opposing aryl groups of the ligand extend into the S1 and S2′ regions, making important but suboptimal interactions with several residues of the binding pocket. Finally, the six-member tetrahydropyrimidine ring appears to point toward solvent space and makes no apparent

Scheme 3[a]

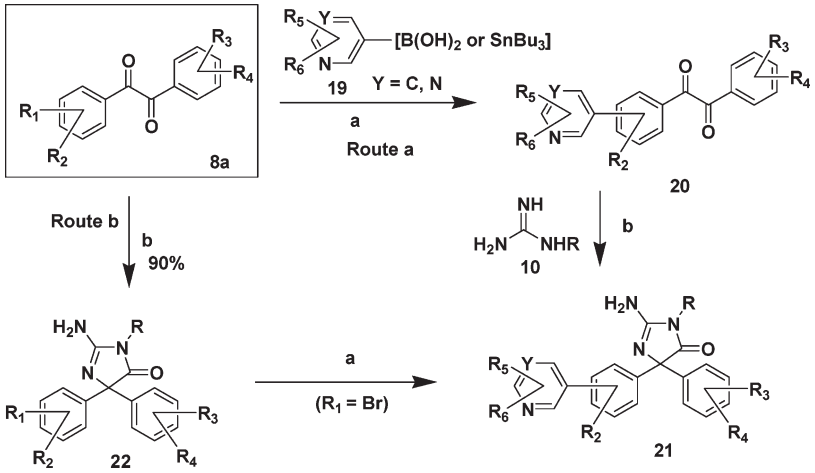

[a] Reagents: (a) arylboronic acid or heteroarylboronic acid or stannates, $(PPh_3)_4$, or $PdCl_2[(o\text{-tolyl})_3P]_2$, toluene or 1,2-diethoxyethane, PPh_3, toluene; (b) $RNH(C{=}NH)NH_2$, K_2CO_3 or Na_2CO_3, EtOH or dioxane or DMF, H_2O.

Table 1. Diphenylaminohydantoins

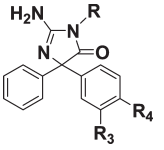

				IC$_{50}$ (μM)[a]			EC$_{50}$ (μM)[a]
compd	R	R$_3$	R$_4$	BACE1	BACE2	cathepsin D	ELISA
3	Me	H	H	3.44 ± 0.29	0.77 ± 0.14	36% at 100 μM	3.4 ± 2.04
23	Et	H	H	25% at 5 μM	5.16 ± 1.95	33% at 100 μM	8.13 ± 2.9
24	H	H	H	14% at 5 μM	87.19	13% at 100 μM	23.5 ± 2.2
25	Me	OMe	H	3.47 ± 0.93	1.19 ± 0.66	46% at 100 μM	5.9 ± 2.9
26	Me	Cl	H	2.50 ± 0.37	0.42	69.18	6.97 ± 3.3
27	Me	H	OMe	3.10	1.72	3% at 100 μM	3.35 ± 1.24
28	Me	H	Cl	2.25 ± 0.03	1.84 ± 0.03	38.18 ± 1.13	2.13 ± 0.67

[a] IC$_{50}$ and EC$_{50}$ values are the mean values of at least two experiments ± SD. Values without SD are for a single determination only.

Table 2. Adamantylaminohydantoins

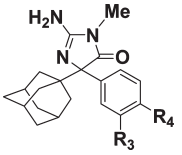

			IC$_{50}$ (μM)[a]			EC$_{50}$ (μM)[a]
compd	R$_3$	R$_4$	BACE1	BACE2	cathepsin D	ELISA
29	H	H	1.53 ± 0.06	0.83 ± 0.24	27.28	0.93 ± 0.2
30	H	OMe	0.16 ± 0.02	0.68 ± 0.16	15.32 ± 2.6	0.044 ± 0.039
(*S*)-**30**	H	OMe	0.07 ± 0.02	0.23 ± 0.03	13.37 ± 0.2	0.07 ± 0.003
(*R*)-**30**	H	OMe	50% at 5 μM	50% at 25 μM	20.78	1.2 ± 0.22
31	H	OEt	0.33 ± 0.07	2.53 ± 0.6	11.53	0.38 ± 0.3
32	H	O-n-Bu	0.87 ± 0.14	5.55 ± 0.56	8.4 ± 1.78	0.57 ± 0.12
33	H	OCF_3	0.47 ± 0.1	3.87 ± 0.9	6.22 ± 1.7	0.9 ± 0.4
34	Me	OMe	0.27 ± 0.07	6.29 ± 2.2	11.1 ± 4	0.23 ± 0.07
(*S*)-**34**	Me	OMe	0.17 ± 0.04	4.02 ± 0.5	9.21	0.13 ± 0.01
(*R*)-**34**	Me	OMe	45	73.58	13.14	1.9 ± 0.04
35	Et	OMe	0.28	4.33	14.10	0.76 ± 0.2
36	OMe	OMe	0.27 ± 0.04	9.59 ± 0.84	36.6 ± 14	0.19 ± 0.08

[a] IC$_{50}$ and EC$_{50}$ values are the mean values of at least two experiments ± SD. Values without SD are for a single determination only.

Table 3. Pyridineaminohydantoins

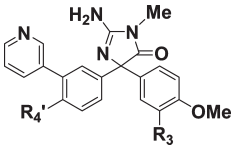

			IC$_{50}$ (μM)[a]			EC$_{50}$ (μM)[a]
compd	R$_3$	R$_4$′	BACE1	BACE2	cathepsin D	ELISA
37	Me	H	0.04 ± 0.01	0.78 ± 0.26	12.5 ± 3.3	0.12 ± 0.05
38	OMe	H	0.09 ± 0.04	4.17 ± 1.4	23.1 ± 7.3	0.9 ± 0.4
39	OEt	H	0.05 ± 0.01	0.6 ± 0.02	10.3 ± 1.9	0.52 ± 0.08
40	OPr	H	0.05 ± 0.03	0.2 ± 0.1	10.1 ± 1.7	0.68 ± 0.3
41	OBu	H	0.05 ± 0.04	0.17 ± 0.01	8.18 ± 1.5	0.67 ± 0.2
42	O-*i*-Pr	H	0.06 ± 0.04	1.84 ± 0.9	12.2 ± 1.4	0.87 ± 0.3
43	O-cyclopentyl	H	0.07 ± 0.01	0.3 ± 0.07	8.3 ± 1.1	0.67 ± 0.1
44	cyclopentyl	H	0.12 ± 0.02	0.96 ± 0.09	1.87 ± 0.13	0.63 ± 0.3
45	F	H	0.05 ± 0.01	0.52 ± 0.1	5.2 ± 1.2	0.42 ± 0.15
46	Cl	H	0.036 ± 0.01	0.56	6.28	0.19 ± 0.05
47	CF$_3$	H	0.04 ± 0.01	1.0 ± 0.01	3.51 ± 0.09	0.29 ± 0.56
48	CN	H	0.15 ± 0.01	0.55 ± 0.2	7.3 ± 1.4	4.5 ± 0.51
49	Me	Me	0.13 ± 0.1	0.96 ± 0.2	2.47 ± 0.29	0.23 ± 0.06
50	Me	CN	0.63 ± 0.08	2.32 ± 0.08	2.19 ± 0.18	1.75 ± 0.3

[a] IC$_{50}$ and EC$_{50}$ values are the mean values of at least two experiments ± SD. Values without SD are for a single determination only.

Table 4. Bicyclic Aminohydantoins

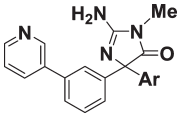

Compd	Ar	BACE1 IC$_{50}$ (μM)[a]	BACE2 IC$_{50}$ (μM)	cathepsin D IC$_{50}$ (μM)	ELISA EC$_{50}$ (μM)[a]
51		0.12	1.13	23.92	0.37±0.16
52		0.25	0.54	21.44	0.68±0.3
53		0.09±0.01	0.5±0.09	10.9±2.3	0.86±0.14

[a] IC$_{50}$ and EC$_{50}$ values are the mean values of at least two experiments ± SD. Values without SD are for a single determination only.

significant contacts with residues of the binding pocket. It was quickly discovered that truncation of the tetrahydropyrimidine, which led to the aminohydantoin **3** (Figure 1), possessed a 10-fold enhancement in potency at the target (IC$_{50}$ = 3.4 μM). The subsequent docking of ligand **3** to the X-ray crystal structure of **2** bound to BACE1 revealed an excellent superposition between these two structures, with both ligands making similar contacts with residues of the binding pocket. The increased affinity of ligand **3** is most likely attributed to the increased acidity of the aminoimidazolone pharmacophore of ligand **3** (**3** pK_a = 5.7 vs **2** pK_a = 7.6), which we hypothesize affects the strength of the hydrogen-bonding interactions between the ligand and catalytic-site aspartic acids.

Armed with this important structure based design data, we investigated the ligand/protein interactions proximal to the catalytic region of the protein. Replacing the *N*-methyl group of the aminohydantoin **3** with the bulkier ethyl group (entry **23**, Table 1) resulted in a noticeable decrease in ligand potency. The amino group of ligand **3** participates in a key interaction with the catalytic-site aspartic acid Asp228, which appears to have been adversely affected by the bulkier ethyl group in this very important pocket and as a result has affected the ligand potency. However, replacement of the *N*-methyl group with the smaller hydrogen nucleus (**24**) also resulted in significant loss of potency. Compound **24** would most likely exist predominantly in the enol form (2-amino-4*H*-imidazol-5-ol), as opposed to the N-methylated derivative, which would occupy a more ketomeric form of the tautomeric pair. This keto−enol shift would have profound implications on not only the pK_a of the heterocycle but also the hydrogen bonding ability of the moiety, resulting in a less favorable interaction.

A significant effort was launched to examine the effects of the substituents on the phenyl moiety that projects to the S2′ pocket. Toward that end, the introduction of either electron donating or withdrawing groups at the meta- and/or para-position of this phenyl moiety resulted in only a marginal improvement of potency (**25**−**28**).

Concomitant with these investigations, we undertook optimization of the S1 pocket binding affinity. Close examination of the BACE1/**2** crystal structure revealed that the S1 pocket is highly hydrophobic and approximately spherical in shape. We hypothesized that increasing the ligand size and lipophilicity to more completely occupy this region would result in increased ligand affinity. To that end, replacement of the S1 phenyl moiety with the bulkier and more lipophilic adamantyl group (**30**, Table 2) resulted in a nearly 20-fold increase in potency (**30** vs **27**) supporting this hypothesis. As will be discussed below, the X-ray structures of ligands **29** and **34** bound to the enzyme have confirmed the orientation of the

Table 5. Substituted Pyridineaminohydantoins

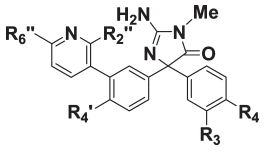

						IC$_{50}$ (μM)[a]			
compd	R_3	R_4	R_4'	R_2''	R_6''	BACE1	BACE2	cathepsin D	EC$_{50}$ (μM)[a] ELISA
54	Me	OMe	H	F	H	0.02 ± 0.002	0.78 ± 0.17	2.58 ± 0.83	0.11 ± 0.01
55	Me	OMe	F	F	H	0.04 ± 0.02	1.84 ± 0.13	2.41 ± 0.17	0.06 ± 0.01
(*S*)-**55**	Me	OMe	F	F	H	0.01 ± 0.002	0.81 ± 0.23	0.82 ± 0.17	0.02 ± 0.01
(*R*)-**55**	Me	OMe	F	F	H	0.56 ± 0.2	1.64 ± 0.12	2.71 ± 0.23	1.2 ± 0.3
56	H	OCF_3	H	F	H	0.06	2.48	3.15	0.37 ± 0.08
57	H	OCF_3	H	OMe	H	0.52 ± 0.08	5.99 ± 0.5	2.05 ± 0.6	2.57 ± 0.9
58	H	OCF_3	H	H	OMe	0.9 ± 0.16	2.51 ± 0.9	4.43 ± 0.4	4.84 ± 1.8

[a] IC$_{50}$ and EC$_{50}$ values are the mean values of at least two experiments ± SD. Values without SD are for a single determination only.

Table 6. Pyrimidineaminohydantoins

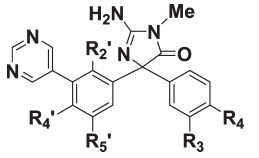

						IC$_{50}$ (μM)[a]			
compd	R_3	R_4	R_2'	R_4'	R_5'	BACE1	BACE2	cathepsin D	EC$_{50}$ (μM)[a] ELISA
59	Me	OMe	H	H	H	0.03 ± 0.01	1.59 ± 0.6	14.3 ± 5.4	0.08 ± 0.04
60	Me	OMe	H	F	H	0.02 ± 0.001	2.8 ± 0.7	6.7 ± 1.6	0.04 ± 0.01
61	H	OCF_3	H	F	H	0.04 ± 0.01	9.69 ± 2.0	4.18 ± 0.8	0.27 ± 0.04
(*R*)-**61**	H	OCF_3	H	F	H	0.02 ± 0.004	7.54 ± 0.7	2.33 ± 0.4	0.07 ± 0.02
(*S*)-**61**	H	OCF_3	H	F	H	1.39	9.97	11.57	2.8 ± 0.07
62	H	OCF_3	H	H	F	0.32 ± 0.07	1.26 ± 0.07	8.55 ± 0.9	
63	H	OCF_3	F	H	H	1.36 ± 0.08	5.04 ± 0.4	26.18	2.83 ± 0.6

[a] IC$_{50}$ and EC$_{50}$ values are the mean values of at least two experiments ± SD. Values without SD are for a single determination only.

Table 7. Pepsin and Renin Inhibition of Representative Compounds

	IC$_{50}$ (μM)[a]	
compd	pepsin	renin
3	11.1 ± 0.4	9.6 ± 1.8
30	14.4 ± 0.3	53.3 ± 2.3
34	15.0 ± 1.4	59.5 ± 2.3
37	19.6 ± 1.7	93.4 ± 1.4
55	66.3 ± 1.2	23.2 ± 1.3
59	33.3 ± 1.4	42.3 ± 3.6
60	35.3 ± 1.1	57.6 ± 1.6
62	35.1 ± 0.7	13.8 ± 0.7

[a] IC$_{50}$ values are the mean values of at least two experiments ± SD.

adamantyl moiety at the enzyme's S1 pocket, as intended. The well-defined orientation of the adamantyl-bearing ligand within the binding pocket, and new insights gained from this structure, directed us to re-evaluate the effects of substituting the phenyl ring of **30**, described earlier, that projects into the S2′ pocket. Increasing the chain length of the para-substituent on the phenyl moiety resulted in 2- to 5-fold potency loss (**31**, **32** vs **30**). Furthermore, the more electronegative trifluoromethoxy group had weaker activity (**33** vs **30**), giving us additional insights into the requirements for binding to the S2′-pocket. Next, we further probed the restrictions on size in the S2′-pocket by employing multiple substituents at the phenyl moiety that project into the pocket. While disubstitutions at the meta- and para-position of the phenyl moiety have resulted in only a slight decrease in ligand potency, this has produced an unexpected increase (∼20- to 30-fold) of the ligand's selectivity against BACE2 (**34**−**36** vs **30**). This intriguing finding prompted us to cocrystallize compounds **29** and **34** with BACE1 in an attempt to explain the role of these substitutions on the ligand's selectivity against BACE2. Overlapping of the X-ray crystal structures of compounds **29** and **34** bound to the enzyme indicated a nearly perfect superimposition of these two ligands (Figure 3). Close examination of the overlapping structures, however, has revealed a shift of the "flap" loop region of the protein backbone of the enzyme, orienting Tyr71 at an open position (approximately 5 Å shift vs apo-position) for the more selective compound **34**. With the unsubstituted ligand **29**, the loop is in a more closed orientation (apo-position), which may explain the selectivity versus BACE2. The open orientation of the "flap" region in the BACE1/**34** structure is perhaps attributed to the steric influence exerted by the meta-methyl group of the S2′-phenyl moiety. The question then became, "How does this substituent interact with the loop in the BACE 2 enzyme structure?" Examination of the protein amino acid sequences of the "flap"

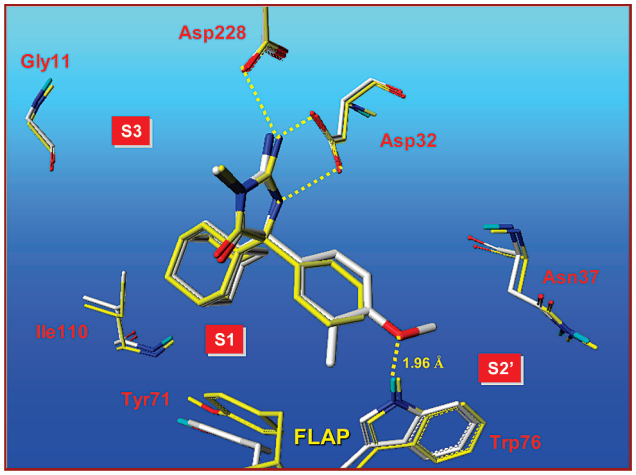

Figure 3. Crystal structures of BACE1 complexed with **29** (shown in yellow) and (*S*)-**34** (shown in white) are overlaid. Movement of Tyr71 from the closed position in complex **29** to the open orientation in complex with (*S*)-**34** is shown. Key hydrogen bonding interactions between ligand and protein at the catalytic aspartic acids Asp32 and Asp228 and at Trp76 of the S2′ region are highlighted with yellow dashed lines.

loops of the BACE1 and BACE2 proteins (overlay of BACE1/2 complex with BACE2 protein homology model not shown) revealed a single amino acid difference (Pro70 in BACE1 is replaced with Lys70 in BACE2) in proximity to the bound ligand. This amino acid difference together with the dynamic motion of the "flap" loop upon ligand engagement apparently influences the ligand/protein contacts and impedes the ligand's affinity for the BACE2 site, thus resulting in increased selectivity.

In addition, the apparent hydrogen-bonding interaction between the para-methoxy group of the phenyl moiety of **34** projecting into the S2′ pocket and residue Trp67 of the BACE1 enzyme backbone is illustrated in the X-ray crystal structure. This key ligand/protein contact can possibly explain the near 10-fold increase in potency of the methoxy-substituted ligand **30** compared to the unsubstituted analogue **29**.

Furthermore, an investigation of the chiral preference of the racemic mixtures of this class of compounds, once separated, showed a clear preference for the *S*-enantiomer (see (*S*)-**30** vs (*R*)-**30**). This was apparent as the crystal structures and modeling studies bore this out. For the less active enantiomer, one could envision keeping the adamantyl and aryl groups in their designed pockets, but in so doing, the aminohydantoin would be flipped into an unfavorable confirmation and pressed into the backbone of the active site of the enzyme. An alternative binding pose of ligand **30** within the binding pocket by flipping the respective P1 and P2′ side chains while retaining the interactions of the aminohydantoin moiety with the catalytic aspartic acids would result in much less interactions with the site compared to (*S*)-**30**. As a result, it could be reflected in the 31-fold potency loss for the (*R*)-**30** enantiomer.

Finally, the cell-based activity of the adamantyl analogues also tracked well with their increased molecular binding with EC_{50} values of 7−200 nM in the ELISA assay. Noteworthy also is that most adamantyl compounds exhibited low potency for cathepsin D with $IC_{50} > 10\ \mu M$.

The next approach in the SAR study was to build off the adamantyl moiety directly toward the unoccupied S3 pocket to improve ligand affinity as was suggested by the BACE1/**34** X-ray crystal structure and molecular modeling calculations. However, functionalizing the adamantyl nucleus in such a way was synthetically challenging, and thus, we had decided to change strategy and use a diphenyl aminohydantoin, such as **27**, as the starting point to explore this objective. The docking of ligand **27** to the X-ray crystal structure of the adamantyl **34** bound to the enzyme indicated that building off the meta-position of the phenyl moiety that projects into the S1-pocket would allow for projection directly toward the unoccupied S3 region (Figure 4). Additionally, X-ray structures together with modeling studies have proposed that a pyridine and/or pyrimidine moiety "hinged" into the polar groove (Gly11, Gly230, and Ser229) located near the catalytic site may favorably interact with the BACE enzyme backbone and improve ligand potency. To that end, we had introduced the pyridine nucleus at the meta-position of the phenyl moiety that led to 70-fold improvement in potency (**37** vs **27**), confirming this hypothesis. To further support our modeling calculations, **37** was then cocrystallized with BACE1, and as shown in Figure 5, the pyridine moiety projects deep into the S3 pocket and makes a water-bridge contact with Ser229 through the buried water found near the catalytic site of the enzyme. This water-bridge contact together with the additional van der Walls contacts between the ligand and enzyme backbone at the S3 region can possibly explain the ligand's increased potency. In addition, the crystal structure shows that the ligand makes several other key hydrogen-bonding interactions with residues (Trp76, Asp32, and Asp228) in the S2′ and catalytic-site pockets. Taken together, this constellation of contacts between the ligand and enzyme effectively "locks" it in place within the rather large BACE1 binding pocket. This potent ligand with multiple contacts offers the opportunity to further refine the aspects of the ligand binding. Interestingly, the para-pyridine analogue (4-pyridyl derivative of **37**) was some 17-fold weaker than the corresponding meta-substituted ligand **37**. While it is difficult to rationalize such a steep reduction of the ligand's potency by the loss of a single water-bridge contact, re-examination of the BACE1/**37** structure revealed an unfavorable electrostatic repulsion involving the electron rich nitrogen of the pyridine nucleus of 4-pyridyl nucleus (when docked into the enzyme site) and the carbonyl oxygen of Gly11 at the enzyme's backbone. Further exploration of this pocket (i.e., electron withdrawing or electron donating groups, multiple examples) had resulted in only marginal improvements in ligand potency, with the exception of the methoxy groups adjacent to pyridine's nitrogen, which showed about a 5-fold decrease in potency (**57** and **58** vs **56**, Table 5). It is hypothesized that the bulkier methoxy group could have adversely affected the water-bridge interaction between the pyridine and residue Ser229 of the S3 pocket. Also, molecular modeling studies (not shown) indicated that the bulkier methoxy group could not be accommodated in this space very well, thus affecting the ligand's potency. Wholesale replacement of the pyridine nucleus of ligand **37** with a phenyl nucleus (not shown) resulted in about 5-fold reduction in ligand potency, indicative of this crucial role of the water-bridge interaction between the ligand and Asp229.

Confident that ligands such as **37** are anchored in place by the multiple hydrogen-bonding interactions and the biaryl moiety occupying the S1−S3 pocket, we focused our efforts to further refine the ligand's binding interactions at the S2′ and S1 regions. To that end, we examined the substitution of electron withdrawing or donating groups at either

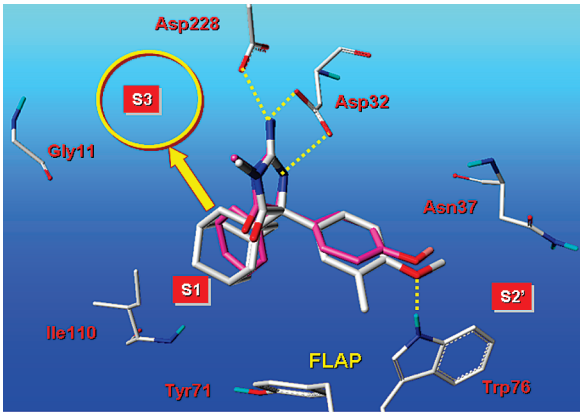

Figure 4. Crystal structure of BACE1 complexed with (*S*)-**34** (shown in white) and **27** (shown in magenta) are overlaid. Key hydrogen bonding interactions between ligand and protein at the catalytic aspartic acids Asp32 and Asp228 and at Trp76 of the S2′ region are highlighted with yellow dashed lines.

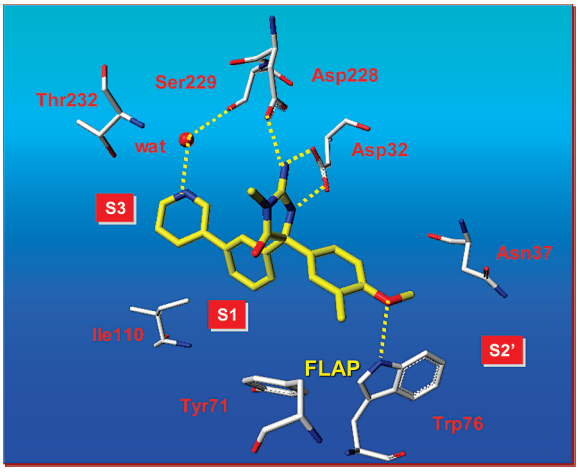

Figure 5. Crystal structure of BACE1 complexed to **37** highlighting the key hydrogen-bonding interactions between the catalytic aspartic acids Asp32 and Asp228, Trp76 at the S2′ region, and water-bridge to Ser229.

the meta- or para-position of the phenyl group located in the S2′ pocket. In all examples, the ligand potency was only minimally affected (~2×) (entries **38**−**48**, Table 3). However, in stark contrast to the BACE1 enzyme SAR, the ligand affinity for BACE2 with these substituted derivatives was more variable. The dimethoxy analogue (**38**) exhibited the highest selectivity (46-fold) against BACE2, while the longer-chained groups, which extended deep into the S2′ pocket, were the least selective compounds (**39**−**44**). These findings are in agreement with the observations described earlier for the adamantyl aminohydantoins. In an attempt to further improve the potency of these 3,4-disubstituted S2′ analogues, we prepared several examples of derivatives that possess a somewhat rigidified substituent pattern that extends into the S2′ region. Compounds **51**−**53** (Table 4), were found to be (2−6)× less potent than **37**, showing how intolerant the S2′ pocket can be to modest changes.

Focusing our attention once again back to the unprime side of the scissile bond, specifically the S1 pocket, it was observed that substitutions at the para-position of the proximal phenyl moiety occupying this region with either a methyl (**49**) or cyano (**50**) group have resulted in an approximate 3- to 16-fold decrease in ligand potency. This decrease in potency is most certainly due to the steric conflict between the ligand and the enzyme backbone residues of the S1 pocket. This hypothesis is not without structure based support, as molecular modeling studies and the BACE1/**37** X-ray crystal structure are in alignment. Noteworthy is that the cell-based activity of the pyridine analogues also tracked well with their increased molecular binding, with EC_{50} values in the range of 20−300 nM in the requisite ELISA assay.

To further expand the scope and breadth of the SAR described already, the pyrimidine analogues (**59**−**63**, Table 6) were prepared. It is quite reasonable to consider that the pyridine ring located in the S3 region (i.e., **37**) can undergo free rotation placing the pyridine nitrogen at a position opposite to the buried water located at the S3 pocket. If this were to happen, the favored water-bridge interaction with Ser229 would be lost. By substituting the pyrimidine ring, we have effectively prevented that occurrence. However, the pyrimidine analogues prepared were only slightly better than the analogous pyridine analogues. Nevertheless, the examples had an unexpectedly improved selectivity against both the highly conserved BACE2 and cathepsin D enzymes. Retrospective examination shows that there are two amino acid differences in the S3 region between BACE1 and BACE2 (BACE1 Asn295 is replaced by Leu in BACE2, and BACE1 Gln11 is replaced by Arg in BACE2). In addition, the S3 pocket of the cathepsin D enzyme is smaller than that of BACE1 and overlaps, in part, with the region occupied by the conserved S3−water of the BACE1 enzyme (not shown). Even though both the pyrimidine and pyridine groups can be considered equal in size, their distinct electronic makeup together with the residue differences at this region of the enzymes could account for the ligand's affinity divergence.

Finally, we have briefly examined the effect on the introduction of fluorine atoms at positions 2, 4, and 5 of the phenyl moiety located at the S1 pocket. The potential for improved potency was a nascent consideration, as we were attempting to identify compounds with improved pharmacokinetic profiles, as this ring was the focus of significant cytochrome P450 metabolism. The details of this investigation will not be discussed here other than to say that significantly improved ligands were realized with this approach. From a potency perspective, while a fluorine group at position 4 only slightly affected the ligand affinity (**60** vs **59**), substitutions at positions 2 and 5 had produced marked reductions (10- to 19-fold) in BACE1 affinity (**62** and **63** vs **61**). Considering that fluoro substituents do not significantly alter the size of the molecule, electrostatic repulsions involving the fluorine groups are the likely cause for the loss of potency. Pyrimidine (*R*)-**61** showed excellent selectivity against BACE2 (> 370-fold). To further explore this finding, ligand (*R*)-**61** was cocrystallized with BACE1 (Figure 6). The examination of the BACE1/(*R*)-**61** structure revealed that the pyrimidine moiety of the ligand makes a water-bridge contact with Ser229, similar to that of the pyridine moiety, while the ligand's phenyl moiety that projects into the S2′ pocket makes hydrogen-bonding-like contacts between the fluorine atoms of the trifluoromethyl group and the enzyme's backbone residues Arg128 and Asn37. The "flap" loop region of the protein backbone orients at a closed position similar to the apo structure. Examination of the amino acid sequences of both BACE1 and BACE2 at this region revealed an amino acid difference between BACE1 and BACE2 (BACE1 Arg128 is replaced by Lys in BACE2) that might play a critical role in the ligand's affinity.

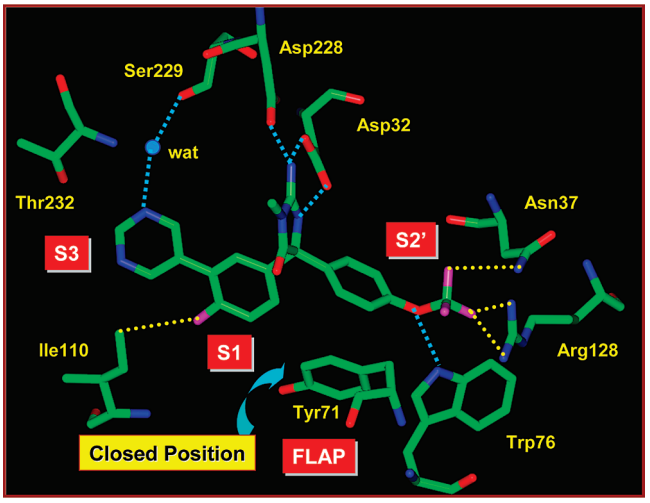

Figure 6. Crystal structures of BACE 1 complexed with (*R*)-**61** highlighting the key hydrogen bonding interactions between ligand and protein at the catalytic aspartic acids Asp32 and Asp228, Trp76 and Arg128 of the S2′ region, Ille110 of the S1 region, and the water-bridge with Ser229. The FLAP sits in the closed position. Water's position is an approximate depiction.

To confirm the specificity of the aminohydantoins for the BACE1 enzyme, a representative set of compounds was evaluated for inhibition of the closely related renin and pepsin aspartyl proteases. As shown in Table 7, all compounds tested demonstrated weak inhibition for both of these targets.

To further elucidate the ability of these ligands to reduce Aβ, an advanced example from this class, (*S*)-**55**, was evaluated in the Tg2576 mice in vivo model for lowering plasma and brain Aβ_{40}.[42] Acute administration of (*S*)-**55** at 100 mg/kg po resulted in a significant 69% reduction of plasma Aβ_{40} measured at the 8 h time point ($p < 0.001$). Significant reduction of brain Aβ_{40} was not observed at this dose because of the limited brain exposure of this compound. Significant focus has been dedicated to improving the central exposure of these ligands while maintaining the robust affinity for the enzyme site demonstrated in this report. Detailed studies exploring and expanding the potential of this class of BACE1 inhibitors will be the subject of a later disclosure.

Summary

In this report, we have described for the first time the detailed exploration of the 5,5-disubstituted aminohydantoin scaffold that led to the discovery of highly potent and selective BACE1 inhibitors. Key analogues demonstrate low nanomolar potency for BACE1 in a FRET assay and exhibit comparable activity in a cell-based (ELISA) assay. In addition, these aminohydantoins show >100× selectivity for the other structurally related aspartyl proteases BACE2, cathepsin D, renin, and pepsin.

Our design strategy followed a traditional SAR approach and was supported by molecular modeling studies based on the cocrystal structure of the HTS-hit **3** in the BACE1 active site. This approach enabled us to rapidly explore the large ligand binding pocket of BACE1 and identify three key protein−ligand interactions at the S2′ and S3 pockets and with the catalytic binding domain (Asp32 and Asp228) that contributes to the ligand potency. Two distinct binding modes between the ligand and the target enzyme were also recognized to contribute to their selectivity against the related BACE2 and cathepsin D aspartyl proteases. An optimized derivative, (*S*)-**55**, displayed an IC_{50} value for BACE1 of 10 nM, cellular EC_{50} activity of 20 nM, and >80-fold selectivity over the other tested aspartyl proteases. Acute oral administration of (*S*)-**55** at 100 mg/kg resulted in a 69% reduction of plasma Aβ_{40} at 8 h in a Tg2576 mouse ($p < 0.001$).

Experimental Section

Chemistry. Melting points were determined in open capillary tubes on a Mel-Temp-II apparatus, and reported uncorrected. ^{1}H NMR spectra were determined in the cited solvent on a Varian Unity or Varian Inova (300−400 MHz) instrument, with tetramethylsilane as an internal standard. Chemical shifts are given in ppm, and coupling constants are in hertz. Splitting patterns are designated as follows: s, singlet; br s, broad singlet; d, doublet; t, triplet; q, quartet; m, multiplet. Mass spectra were recorded on a Micromass LCT, Waters spectrometer. Elemental analyses (C, H, N) were performed on a Perkin-Elmer 240 analyzer, and all compounds are within ±0.4% of theory unless otherwise indicated. HPLC techniques and high resolution mass spectrometry were used to determine the purity of compounds outside the range of the elemental analysis assessment. Purity of all final products was >96% as determined by HPLC and/or combustion analysis. Purity was determined by HPLC analysis using the following protocols. Method A: mobile phase A, 10 mM ammonium formate in water (pH 3.5); solvent B, 50:50 ACN/MeOH; solvent gradient 85/15 to 5/95 A/B in 2 min, hold 1.25 min, re-equilibrate 0.5 min; flow rate 1.1 mL/min; column, Agilent SB C18 1.8 μM, 3.0 mm × 50 mm; temperature 45 °C; detection at 210−370 nm. Method B: mobile phase B, 10 mM ammonium carbonate in water (pH 9.5); solvent B, 60:50 ACN/MeOH; solvent gradient 85/15 to 5/95 A/B in 2 min, hold 1.25 min, re-equilibrate 0.5 min; flow rate 1.1 mL/min; column Waters Xbridge C18 2.5 μM, 3.0 mm × 50 mm; temperature 45 °C; detection at 210−370 nm. All products, unless otherwise noted, were purified by "flash chromatography" with use of 220−400 mesh silica gel. Thin-layer chromatography was done on silica gel 60 F-254 (0.25 mm thickness) plates. Visualization was accomplished with UV light and/or 10% phosphomolybdic acid in ethanol. The hydration was determined by the Karl Fischer titration, using a Mitsubishi moisture meter model CA-05. Unless otherwise noted, all materials were obtained commercially and used without further purification. All reactions were carried out under an atmosphere of dried argon or nitrogen.

Representative synthetic protocols of the aminohydantoins shown in Schemes 1−3 are described below.

Exemplified Analogues of Scheme 1. Route a. Preparation of 2-Amino-5-(4-methoxyphenyl)-3-methyl-5-tricyclo[3.3.1.1^{3,7}]dec-1-yl-3,5-dihydro-4*H*-imidazol-4-one (10b, A = 1-Adamantyl, R = Me, R$_3$ = H, R$_4$ = OMe). Step b. Lithium bis(trimethylsilyl)amide in THF (1.0 M, 52.3 mL, 52.3 mmol) was added into a stirred suspension of (4-methoxybenzyl)triphenylphosphonium chloride (21.9 g, 52.3 mmol) in THF (100 mL). The mixture was stirred for 15 min at room temperature, cooled to −5 °C, and treated with a solution of tricyclo-[3.3.1.1^{3,7}]decane-1-carbonyl chloride (9.44 g, 47.5 mmol) in THF (20 mL) and stirred for an additional 2 h, while the mixture temperature was gradually raised to room temperature. The mixture was then treated with water (50 mL) and sodium periodate (11.18 g, 52.3 mmol), stirred at 50 °C for 17 h, cooled to room temperature, and diluted with ethyl acetate. The organic phase was separated and washed sequentially with water and brine, dried over sodium sulfate, filtered, and concentrated. Purification of the resultant residue by flash chromatography (silica gel, EtOAc/hexanes, 1/9) afforded 1-(4-methoxyphenyl)-2-tricyclo[3.3.1.1^{3,7}]dec-1-ylethane-1,2-dione (6.85 g, 48%) as a yellow solid. MS *m*/*e* 299 $(M + H)^+$; ^{1}H NMR (300 MHz, $CDCl_3$) δ 2.05−1.55 (m, 15H), 3.89 (s, 3H), 6.96 (d, J = 8.9 Hz, 2H, 7.78 (d, J = 8.9 Hz, 2H).

Step h. A mixture of 1-(4-methoxyphenyl)-2-tricyclo-[3.3.1.1^{3,7}]dec-1-ylethane-1,2-dione (6.71 g, 22.5 mmol) and 1-methylguanidine hydrochloride (11.1 g, 101 mmol) in dioxane (75 mL) and ethanol (100 mL) was stirred at room temperature for 5 min, treated with an aqueous solution of sodium carbonate (10.7 g, 101 mmol; 10 mL of water), heated at 85 °C with stirring for 3.5 h, cooled to room temperature, and concentrated in vacuo. Purification of the resultant residue by flash chromatography (silica, 95:5:0.5 methylene chloride/methanol/concentrated ammonium hydroxide) afforded 2-amino-5-(4-methoxyphenyl)-3-methyl-5-tricyclo[3.3.1.1^{3,7}]dec-1-yl-3,5-dihydro-4*H*-imidazol-4-one as a white solid: 3.41 g (43% yield), mp 150−155 °C; MS *m*/*e* 354 (M + H)$^+$; ^{1}H NMR (300 MHz, $CDCl_3$) and ^{1}H NMR (400 MHz, DMSO-d_6) δ 1.38 (m, 6H), 1.55 (m, 3H), 1.65 (m, 3H), 1.82 (bs,3H), 2.81 (s, 3H), 3.67 (s, 3H), 6.26 (brs, 2H), 6.79 (d, J = 8.85 Hz, 2H), 7.55 (m, J = 8.85 Hz, 2H). Anal. ($C_{17}H_{17}N_3O_2 \cdot 0.2H_2O$) C, H, N.

Generation of the Enantiomers of 10b (R = Me, R_3 = H, R_4 = OMe) Using Chiral HPLC Techniques. Racemic mixture of 2-amino-5-(4-methoxyphenyl)-3-methyl-5-tricyclo[3.3.1.1^{3,7}]dec-1-yl-3,5-dihydro-4*H*-imidazol-4-one was separated to its two enantiomers by HPLC on Chiralcel AD, 0.46 cm × 25 cm using mobile phase EtOH/hexane (1:9 with 0.1% DEA) and a flow rate of 1.0 mL/min to afford the (*R*)- and (*S*)-compounds.

(*S*)-2-amino-5-(4-methoxyphenyl)-3-methyl-5-tricyclo[3.3.1.1^{3,7}]-dec-1-yl-3,5-dihydro-4*H*-imidazol-4-one (A): mp 215 °C; $[\alpha]^{25}$ −17.4 (*c* 1%, MeOH); MS *m*/*e* 352 (M − H)$^-$; ^{1}H NMR (400 MHz, DMSO-d_6) δ 1.38 (m, 6H), 1.55 (m, 3H), 1.65 (m, 3H), 1.82 (bs,3H), 2.81 (s, 3H), 3.67 (s, 3H), 6.26 (brs, 2H), 6.79 (d, J = 8.85 Hz, 2H), 7.55 (d, J = 8.85 Hz, 2H). Anal. ($C_{17}H_{17}N_3O_2 \cdot 0.7H_2O$) C, H, N.

(*R*)-2-Amino-5-(4-methoxyphenyl)-3-methyl-5-tricyclo[3.3.1.1^{3,7}]-dec-1-yl-3,5-dihydro-4*H*-imidazol-4-one: mp 215 °C; $[\alpha]^{25}$ +17.6 (*c* 1%, MeOH); MS *m*/*e* (M − H)$^-$ 352; ^{1}H NMR (400 MHz, DMSO-d_6) δ 1.38 (m, 6H), 1.55 (m, 3H), 1.65 (m, 3H), 1.82 (bs,3H), 2.81 (s, 3H), 3.67 (s, 3H), 6.26 (brs, 2H), 6.79 (d, J = 8.85 Hz, 2H), 7.55 (d, J = 8.85 Hz, 2H). Anal. ($C_{17}H_{17}N_3O_2 \cdot 0.3H_2O$) C, H, N.

Preparation of 2-Amino-5-(4-methoxyphenyl)-3-methyl-5-phenyl-3,5-dihydro-4*H*-imidazol-4-one (10a, A = Ph, R_3 = H, R_4 = OMe, R = Me). Step h. To a mixture of 1-(4-methoxyphenyl)-2-phenylethane-1,2-dione (0.30 g, 1.2 mmol), ethanol (15 mL), and water (4 mL) were added 1-methylguanidine hydrochloride (0.09 g, 1.2 mmol) and K_2CO_3 (0.49 g, 3.6 mmol). The mixture was refluxed for 3 h and then cooled to room temperature, and the volatiles were removed under reduced pressure. The residue was taken in water (50 mL) and extracted with $CHCl_3$. The organic extracts were dried over $MgSO_4$. Evaporation and purification by flash chromatography on silica gel (ethyl acetate as the eluting solvent) produced 2-amino-5-(4-methoxyphenyl)-3-methyl-5-phenyl-3,5-dihydro-4*H*-imidazol-4-one as a white solid (0.29 g, 80% yield). MS *m*/*e* 296 (M + H)$^+$; ^{1}H NMR (DMSO-d_6, 300 MHz) δ 2.97 (s, 3H), 3.71 (s, 3H), 6.59 (b, 2H), 6.84 (d, J = 8.4 Hz, 2H), 7.21 (m, 1H), 7.26−7.35 (m, 4H), 7.41 (d, J = 8.4 Hz, 2H). Anal. ($C_{17}H_{17}N_3O_2 \cdot 0.2H_2O$) C, H, N.

Route b. Preparation of 1-(4-Methoxy-3-methylphenyl)-2-phenylethane-1,2-dione (8a, A = Ph, R, R_3 = Me, R_4 = OMe). Steps f and g. A mixture of oxo(phenyl)acetic acid (2 g, 13.32 mmol), oxalyl chloride (3.89 g, 30.63 mmol), CH_2Cl_2 (30 mL), and *N*,*N*-dimethylformamide (0.005 mL) was stirred at room temperature for 3 h. The volatiles were removed in vacuo, and the residue was taken in THF (20 mL) and added into a cold (0 °C) mixture of bromo(4-methoxy-3-methylphenyl)magnesium (1 M, 15.05 mL, 15.05 mmol), CuBr (1.08 g, 7.51 mmol), LiBr (1.3 g, 15.02 mmol), and THF (30 mL). The mixture was stirred for 30 min, poured into cold HCl (1 N), and extracted with ethyl ether. The organic extracts were dried over $MgSO_4$. Evaporation and purification by flash chromatography (5% EtOAc/hexanes) gave a yellow solid (0.92 g, 33% yield): MS *m*/*e* 254 (M)$^+$; ^{1}H NMR (300 MHz, DMSO-d_6): δ 2.21 (s, 3H), 3.92 (s, 3H), 7.16 (d, J = 8.3 Hz, 1H), 7.62 (m, *2*H), 7.76−7.81 (m, 3H), 7.9 (d, J = 8.24 Hz, 1H).

Preparation of 3-Methyl-4-methoxybenzyltriphenylphosphine Chloride (5, R_3 = Me, R_4 = OMe). Triphenylphosphine (23.29 g, 87.9 mmol) was dissolved in 135 mL of toluene, and 3-methyl-4-methoxybenzyl chloride (15 g, 11.4 mmol) was then added. The mixture was heated to reflux for 3 h and then cooled to room temperature. The solids were collected and washed with a small amount of ether and dried. A white solid (23 g, 66% yield) was recovered. MS *m*/*e* (M)$^+$ 397; ^{1}H NMR (DMSO-d_6, 300 MHz) δ 1.9 (s, 3H), 3.72 (s, 3H), 5.3 (d, 2H), 6.55 (s, 1H), 6.82 (m, 2H), 7.65 (m, 6H), 7.75 (m, 6H), 7.92 (m, 3H).

Exemplified Analogues of Scheme 2. Preparation of 2-Amino-3-methyl-5-phenyl-5-tricyclo[3.3.1.1^{3,7}]dec-1-yl-3,5-dihydro-4*H*-imidazol-4-one (10b, A = 1-Adamantyl, R = Me, R_3 = H, R_4 = OMe). Step a. To a cold (0 °C) solution of benzaldehyde (10.15 mL, 0.1 mol) and triethylphosphite (19.1 mL, 0.1 mol) was added dropwise chlorotrimethylsilane (12.6 mL, 0.1 mol) over a 10 min period. After the addition was complete, the ice bath was removed and the reaction mixture was warmed up to 120 °C for 8 h and distilled (180 °C, 10.0 mmHg) to afford diethyl 1-phenyl-1-(trimethylsilyloxy)methane phosphonate as a colorless oil (25 g, 79% of yield): MS *m*/*e* (M + H)$^+$ 317; ^{1}H NMR (400 MHz, $CDCl_3$) δ 0.08 (s, 9H), 1.22 (m, 6H), 4.01 (m, 4H), 4.97 (d, 1H), 7.32 (m, 3H), 7.44 (m, 2H).

Step b. To a cold (−78 °C) solution of diethyl 1-phenyl-1-(trimethylsilyloxy)methane phosphonate (3.16 g, 10 mmol) in THF was added dropwise lithium diisopropylamide (2 M, 5.25 mL) over a 10 min period. The reaction mixture was stirred for another 30 min, treated with tricyclo[3.3.1.1^{3,7}]decane-1-carbonyl chloride (2.09 g, 10 mmol) in THF, and heated slowly to room temperature overnight. Under cooling the reaction mixture was poured into saturated NH_4Cl solution and extracted with ethyl ether. The extracts were combined, dried over $MgSO_4$, and concentrated in vacuo. The resultant residue was purified by flash chromatography on silica gel (hexanes/EtOAc, 95/5) to afford diethyl {2-oxo-2-phenyl-1-tricyclo[3.3.1.1^{3,7}]dec-1-yl-1-[(trimethylsilyl)oxy]ethyl}phosphonate as a colorless oil (2.1 g, 43% yield, mp 136 °C): MS *m*/*e* (M + H)$^+$ 479.1; ^{1}H NMR (400 MHz, DMSO-d_6) δ 0.21 (s, 9H), 1.13 (t, J = 7.6 Hz, 6H), 1.45−1.82 (m, 15H), 3.91 (dq, J = 7.6 Hz, 4H), 7.30−7.43 (m, 5H).

Step c. A mixture of diethyl {2-oxo-2-phenyl-1-tricyclo-[3.3.1.1^{3,7}]dec-1-yl-1-[(trimethylsilyl)oxy]ethyl}phosphonate (2.1 g, 4.38 mmol), aqueous saturated $NaHCO_3$ (1.5 mL), and MeOH (7 mL) was heated at reflux temperature for 2 h, cooled, acidified with HCl (2.5 mL, 2 N), and extracted with ether. The ether extracts were combined, dried over $MgSO_4$, and concentrated in vacuo. Purification of this residue by flash chromatography on silica gel (hexane/EtOAc, 95/5) gave 1-phenyl-2-tricyclo[3.3.1.1^{3,7}]dec-1-ylethane-1,2-dione as a yellow oil (0.21 g, 18% yield); MS *m*/*e* (M + H)$^+$ 268.15; ^{1}H NMR (400 MHz, DMSO-d_6) δ 1.70 (m, 6H), 1.90 (bs, 6H), 2.02 (m, 3H), 7.62 (m, 2H,), 7.79 (m, 3H).

Step d. A mixture of 1-phenyl-2-tricyclo[3.3.1.1^{3,7}]dec-1-ylethane-1,2-dione (0.21 g, 0.78 mmol), Na_2CO_3 (0.25 g, 2.34 mmol), 1-methylguanidine hydrochloride (0.12 g, 1,01 mmol), and H_2O (0.70 mL) in dioxane (3.5 mL) and EtOH (3.5 mL) was stirred at 80 °C for 18 h and concentrated in vacuo. The resultant residue was dissolved in $CHCl_3$, washed with water, dried over K_2CO_3, and evaporated to dryness. Purification of this residue by flash chromatography on silica gel ($EtOAc/CH_2Cl_2/Et_3N$, 7.5/2/0.5) gave 5-(1-adamantyl)-2-amino-3-methyl-5-phenyl-3,5-dihydro-4*H*-imidazol-4-one as a white solid (0.11 g, 43% yield, mp 250 °C); MS *m*/*e* (M + H)$^+$ 324; ^{1}H NMR (400 MHz, DMSO-d_6) δ 1.40 (m, 6H), 1.50 (m, 3H), 1.70 (m, 3H), 1.85 (bs, 3H), 2.85 (s, 3H), 6.40 (bs, 2H), 7.22 (m, 3H), 7.62 (m, 2H). Anal. ($C_{20}H_{25}N_3O \cdot 0.4H_2O$) C, H, N.

Exemplified Analogues of Scheme 3. Route a. Preparation of 4-[2-Amino-4-(4-methoxy-3-methylphenyl)-1-methyl-5-oxo-4,5-dihydro-1*H*-imidazol-4-yl]-2-pyridin-3-ylbenzonitrile (Stille Coupling, 20, R_3 = Me, R_4 = OMe, R_2 = 4-CN, R_5, R_6 = H, Y = C). Step a. Dichlorobis(tri-*o*-tolylphosphine)palladium(II) (39.6 mg, 0.05 mmol)

was added into a mixture of 2-bromo-4-[(4-methoxy-3-methylphenyl)(oxo)acetyl]benzonitrile (200 mg, 0.56 mmol), 3-(tributylstannyl)pyridine (268 mg, 0.73 mmol), and 1,2-diethoxyethane (6 mL). The reaction flask was immersed into an oil bath of 145 °C, and the mixture was stirred for 30 min and filtered to remove the catalyst. Evaporation and purification by flash chromatography (hexanes/EtOAc, 2/1), and crystallization from ethyl ether/hexanes gave 4-[(4-methoxy-3-methylphenyl)(oxo)acetyl]-2-pyridin-3-ylbenzonitrile as a yellow solid (181 mg, 91% yield): MS *m*/*e* 357 $(M + H)^+$; ^{1}H NMR (400 MHz, DMSO-d_6) δ 2.21 (s, 3H), 3.93 (s, 3H), 7.18 (d, J = 8.69 Hz, 1H), 7.61 (m, 1H), 7.82 (d, J = 8.54, 1H), 7.84 (dd, J = 8.54, 1.99 Hz, 1 H), 8.07 (dd, J = 7.76, 1.67 Hz, 1H), 8.12 (m, J = 1.38 Hz, 2H), 8.25 (d, J = 8.08 Hz, 1H), 8.74 (m, 1H), 8.85 (d, 1.68 Hz, 1H).

Step b. Sodium carbonate (214 mg, 2.02 mmol) in water (2 mL) was added into a mixture of 4-[(4-methoxy-3-methylphenyl)(oxo)acetyl]-2-pyridin-3-ylbenzonitrile (160 mg, 0.45 mmol), 1-methylguanidine hydrochloride (222 mg, 2.02 mmol), dioxane (7 mL), and ethyl alcohol (9 mL). The reaction mixture was stirred at 85 °C for 3 h. The volatiles were removed in vacuo, and the residue was taken in chloroform and washed with water. The organic extracts were dried over $MgSO_4$. Evaporation and purification by flash chromatography (EtOAc/MeOH, 15/1) and crystallization from $CHCl_3$/hexanes gave 4-[2-amino-4-(4-methoxy-3-methylphenyl)-1-methyl-5-oxo-4,5-dihydro-1*H*-imidazol-4-yl]-2-pyridin-3-ylbenzonitrile as a white solid (138 mg, 75% yield): MS *m*/*e* 412 $(M + H)^+$; ^{1}H NMR (400 MHz, DMSO-d_6) δ 2.09 (s, 3H), 2.98 (s, 3H), 3.74 (s, 3H), 6.74 (brs, 2H), 6.86 (d, J = 8.69 Hz, 1H), 7.22 (s, 1H), 7.26 (d, J = 8.54 Hz, 1H), 7.58 (m, 1H), 7.69 (s, 1H), 7.70 (s, 1H), 7.9−8.0 (m, 2H), 8.7 (m, 2H). Anal. ($C_{24}H_{21}N_5O_2 \cdot 0.8H_2O$) C, H, N.

Preparation of 2-Amino-5-(4-methoxy-3-methylphenyl)-5-[3-(pyridin-3-yl)phenyl]-3,5-dihydro-4*H*-imidazol-4-one (Suzuki Coupling, 21, R, R_3 = Me, R_4 = OMe, R_2, R_5, R_6 = H, Y = C). Step b. 1-(3-Bromophenyl)-2-(4-methoxy-3-methylphenyl)-ethane-1,2-dione (0.4 g, 1.2 mmol) was dissolved in 1,4-dioxane (10 m) and water (2 mL). To this was then added 3-pyridineboronic acid (0.18 g, 1.44 mmol) followed by K_2CO_3 (0.38 g, 2.76 mmol). The mixture was heated to 70 °C, and triphenylphosphine (0.018 g, 0.069 mmol) was added followed by palladium acetate (0.0083 g, 0.037 mmol) addition. The mixture was stirred at 100 °C for 16 h, cooled to room temperature, and extracted with $CHCl_3$. The organics washed with 1 N NaOH and water and dried over $MgSO_4$. Evaporation and purification by flash chromatography on silica gel (2:1 ethyl acetate/hexane) gave 1-(4-methoxy-3-methylphenyl)-2-(3-pyridin-3-ylphenyl)ethane-1,2-dione as a yellow solid (0.3 g, 75% yield): MS *m*/*e* $(M)^+$ 332; ^{1}H NMR (DMSO-d_6 300 MHz) δ 2.22 (s, 3H), 3.92 (s, 3H), 7.15 (d, J = 8.39 Hz, 1H), 7.53 (dd, J = 7.93, 3.2 Hz, 1H), 7.75 (d, J = 7.78 Hz, 1H), 7.82 (m, 2H), 7.91 (d, J = 7.78 Hz, 1H), 8.15 (m, 2H), 8.2 (s, 1H), 8.64 (m, 1H), 8.94 (d, J = 1.98 Hz, 1H). Anal. ($C_{23}H_{22}N_4O_2 \cdot 0.5H_2O$) C, H, N.

Route b. Preparation of 2-Amino-5-[4-fluoro-3-(2-fluoropyridin-3-yl)phenyl]-5-(4-methoxy-3-methylphenyl)-3-methyl-3,5-dihydroimidazol-4-one (21, R, R_3 = Me, R_4 = OMe, R_2 = 4-F, R_5 = 2-F, R_6 = H, Y = C). Step b. A mixture of 1-(3-bromo-4-fluorophenyl)-2-(4-methoxy-3-methylphenyl)ethane-1,2-dione (10.4 g, 29.5 mmol) and 1-methylguanidine hydrochloride (14.6 g, 133 mmol) in dioxane (154 mL) and ethanol (154 mL) was stirred at room temperature for 5 min. A solution of sodium carbonate (14.0 g, 133 mmol) in water (62 mL) was then added and the mixture immersed into an oil bath at 85 °C and stirred for 45 min. The reaction mixture was cooled to room temperature and concentrated. Purification by flash chromatography (silica, 95:5:0.5 methylene chloride/methanol/concentrated ammonium hydroxide) afforded 2-amino-5-(3-bromo-4-fluorophenyl)-5-(4-methoxy-3-methylphenyl)-3-methyl-3,5-dihydro-4*H*-imidazol-4-one (10.9 g, 90%) as a white solid: MS *m*/*e* 406 $(M + H)^+$; ^{1}H NMR (300 MHz, CD_3OD) δ 7.59 (dd, J = 6.6, 2.4 Hz, 1H), 7.38 (ddd, J = 8.7, 4.8, 2.4 Hz, 1H), 7.18−7.03 (m, 3H), 6.83 (d, J = 8.7 Hz, 1H), 3.80 (s, 3H), 3.10 (s, 3H), 2.30 (s, 3H).

Step a. A mixture of 2-amino-5-(3-bromo-4-fluorophenyl)-5-(4-methoxy-3-methylphenyl)-3-methyl-3,5-dihydro-4*H*-imidazol-4-one (4.50 g, 11.1 mmol), 2-fluoropyridine-3-boronic acid (2.34 g, 16.6 mmol), sodium carbonate (3.52 g, 33.2 mmol), bis(triphenylphosphino)palladium(II) dichloride (0.389 g, 0.554 mmol), and triphenylphosphine (0.291 g, 1.11 mmol) in 1:1 toluene/EtOH (200 mL) was degassed and heated at 110 °C for 2.5 h. The mixture was cooled to room temperature, concentrated, and purified by flash chromatography (silica, 97:3:0.25 methylene chloride/methanol/concentrated ammonium hydroxide) to afford a 1.78 g batch of 2-amino-5-[4-fluoro-3-(2-fluoropyridin-3-yl)-phenyl]-5-(4-methoxy-3-methylphenyl)-3-methyl-3,5-dihydroimidazol-4-one (2.43 g, 52%) as a white solid: (95:5:0.25 methylene chloride/methanol/concentrated ammonium hydroxide): mp 75−80 °C; MS *m*/*e* 423 $(M + H)^+$; ^{1}H NMR (300 MHz, CD_3OD) δ 8.23 (dt, J = 5.0, 1.0 Hz, 1H), 7.93 (dt, J = 7.5, 1.5 Hz, 1H), 7.51−7.34 (m, 3H), 7.21−7.08 (m, 3H), 6.84 (d, J = 8.0 Hz, 1H), 3.80 (s, 3H), 3.10 (s, 3H), 2.01 (s, 3H). Anal. ($C_{23}H_{20}F_2N_4O_2 \cdot 0.3H_2O$) C, H, N.

Biological Methods. FRET-Based Peptide Cleavage Assays. A homogeneous, continuous fluorescence resonance energy transfer (FRET) was used to assess compound inhibition for BACE1, BACE2, cathepsin D, pepsin, and renin activities.[41] The BACE1 and BACE2 activities were based on the cleavage of peptide substrate Abz-SEVNLDAEFR-Dpa (Swedish substrate), while peptide substrate MOCAc-GKPILFFRLK (Dnp)-D-R-NH_2 was used for cathepsin D and pepsin, and peptide substrate RE(EDANS)-IHPFHLVIHTK(DABCYL)-R was used for renin. Kinetic rates were calculated, and IC_{50} values were determined by fitting the % inhibition as a function of compound concentration to the Hill equation ($y = ((B \times Kn) + (100 \times xn))/(Kn + xn)$).

Cell-Based Aβ Inhibition Assay. CHO-K1 cells recombinantly expressing human wild-type APP (CHO-WT) were grown to confluence and then treated with serum-free medium (Ultraculture) supplemented with test compound in DMSO or DMSO alone (vehicle) at a final [DMSO] of 0.1% (v/v). Conditioned medium was harvested at 24 h and assayed using streptavidin MSD plates, an electrochemiluminescent immunoassay with biotinylated mouse monoclonal antibody 6E10 (Signet, Dedham, MA) was used as capture, and rabbit anti-Aβ_{40} or Aβ_{42} antibodies (Biosource, Camarillo, CA) were used as detection antibodies, with a secondary of MSD ECL tagged sheep antirabbit used for electrochemiluminescent amplification.

Data analysis of the MSD assay was performed by fitting the percent inhibition as a function of compound concentration to a four-parameter logistic curve, and the concentration at which the cellular production of Aβ_{40} or Aβ_{42} was reduced by 50% (EC_{50}) was determined. Compound toxicity was assessed via mitochondrial function using an MTS readout (MTS kit from Promega); values are represented as LD_{50} or the dose of compound that resulted in 50% of control signal (e.g., 50% of the highest MTS signal).

X-ray Crystallography. Cloning/Expression of BACE1. A human BACE1 secreting mammalian secreting cell line (CHO cell line) was made by expressing a construct in which the prodomain plus ectodomain of human BACE1 (residues 22−454) was fused to the honeybee melittin secretory leader sequence at the 5′ end, and the Fc region of IgG, separated from the BACE sequence via an enterokinase cleavage site, was fused at the 3′ end of BACE1. The BACE1/Fc fusion protein was affinity purified by protein-A sepharose, and removal of the Fc domain was achieved with enterokinase cleavage. Purified BACE1 protein was accomplished via sequential size-exclusion chromatography. *E. coli*-derived expression material was used for cocrystallographic studies. A codon-derived BACE1 *E. coli* expression construct was fused to a carboxy-terminal 6× HIS tag. After scale-up, inclusion bodies were purified and

protein was refolded and dialyzed. The prodomain was cleaved with furin, and BACE1 was further purified by size exclusion chromatography. The refolded *E. coli* derived BACE1 showed the same enzymatic activity as the CHO-derived material (data not shown).

Crystallization and X-ray Diffraction Analysis of BACE1. Crystals were grown by hanging drop vapor diffusion at 18 °C in drops containing 1.0 μL of protein stock solution (200 μM protein, 20 mM Tris-HCl, pH 7.5, 250 mM NaCl, and 240 μM compound of interested diluted from a 100 mM stock in DMSO) mixed with 1.0 μL of well solution (6% PEG 3350, 0.1 M sodium acetate, pH 5.4) and equilibrated against 0.5 mL of well solution. Rod shaped crystals grew in several days.

Data Collection. Crystals were drawn through a solution of 25% glycerol and 75% well solution and cooled rapidly in liquid nitrogen. Diffraction data were recorded at the ALS beamline 5.0.1 on a q-210 CCD camera. Intensities were integrated and scaled using the programs Denzo and Scalepack.[43]

Phasing, Model Building and Refinement. Structures were determined by molecular replacement using AmorE[44] and the apo structure of BACE1 (PDB code 1W50) as the search model. The final structures were obtained after several iterative cycles of refinement using Phenix[45] and model improvement in Coot.[46]

Data Deposition. The atomic coordinates of the BACE1 crystal structure for compounds **2** (3IGB),[41] **29** (3IND), (*S*)-**34** (3INE), **37** (3INF), and (*R*)-**61** (3INH) have been deposited in the Protein Data Bank, Research Collaboratory for Structural Bioinformatics, Rutgers University, New Brunswick, NJ.

Molecular Modeling. Docking calculations were performed using the QXP software package.[47] Once the X-ray ligands were minimized in the active site, constrained simulated annealing calculations were performed to relieve any artifacts of the X-ray refinement perceived as unfavorable interactions or strain by the modified AMBER force field with QXP. The X-ray ligand was then redocked to confirm that the lowest energy pose is in agreement with the X-ray structure. Once the binding site model was generated, docking of analogues was performed using the QXP Monte Carlo docking algorithm MCDOCK in combination with CombiDOCK. Visualization of X-ray structures and docking results was performed using the Insight II software package (www.accelrys.com, Accelrys, Inc., San Diego, CA). Conformational analysis was performed using Macromodel (Macromodel 8.0; Schrodinger, LLC, Portland, OR), with the OPLS-AA force fields, and a GBSA solvation model.

Note Added after ASAP Publication. This paper was published on the web on December 7, 2009 with an error in Data Deposition. The revised version was published on January 5, 2010.

Supporting Information Available: X-ray crystallographic data (collection details, refinement statistics), ^{1}H NMR and analytical data of intermediates and final compounds not listed in the Experimental Section, and supplemental information of biological assays. This material is available free of charge via the Internet at http://pubs.acs.org.

References

(1) Selkoe, D. J. Alzheimer disease: mechanistic understanding predicts novel therapies. *Ann. Intern. Med.* **2004**, *140*, 627–638.

(2) Alloul, K; Sauriol, L.; Kennedy, W.; Laurier, C.; Tessier, G.; Novosel, S.; Contandriopoulos, A. Alzheimer's disease: a review of the diseas, its epidemiology and economic impact. *Arch. Gerontol. Geriatr.* **1998**, *27*, 189–221.

(3) (a) Enz, A.; Amstutz, R.; Boddeke, H.; Gmelin, G.; Malanowski, J. Brain selective inhibition of acetylcholineesterase: a novel approach to therapy for Alzheimer's disease. *Prog. Brain Res.* **1993**, *98*, 431–438. (b) Fillit, H.; Hill, J. Economics of dementia and pharmacoeconomics of dementia therapy. *Am. J. Geriatr. Pharmacother.* **2005**, *3*, 39–49.

(4) Arendt, T. Alzheimer's disease as a disorder of mechanisms underlying structural brain self-organization. *Neuroscience* **2001**, *102*, 723–765.

(5) Dickson, D. W. The pathogenesis of senile plaques. *J. Neuropathol. Exp. Neurol.* **1997**, *56*, 321–339.

(6) (a) Selkoe, D. J. Alzheimer's disease: genotypes, phenotypes, and treatments. *Science* **1997**, *275*, 630–631. (b) Hardy, J.; Selkoe, D. J. The amyloid hypothesis of Alzheimer's disease: progress and problems on the road to therapeutics. *Science* **2002**, *297*, 353–356.

(7) Vassar, R.; Citron, M. Aβ-generating enzymes: recent advances in β- and γ-secretase research. *Neuron* **2000**, *27*, 416–422.

(8) Selkoe, D. J. Alzheimer's disease: genes, proteins, and therapy. *Physiol. Rev.* **2001**, *81*, 741–766.

(9) Hussain, I.; Powell, D.; Howlett, D. R.; Tew, T. G.; Meek, T. D.; Chapman, C.; Gloger, I. S.; Murphy, K. E.; Southan, C. D.; Ryan, D. M.; Smith, T. S.; Simmons, D. L.; Walsh, F. S.; Dingwall, C.; Christie, G. Identification of a novel aspartic protease (Asp2) as β-secretase. *Mol. Cell. Neurosci.* **1999**, *14*, 419–427.

(10) Lin, X.; Koelsch, G.; Wu, S.; Downs, D.; Dashti, A.; Tang, J. Human aspartic protease memapsin 2 cleaves the β-secretase site of β-amyloid precursor protein. *Proc. Natl. Acad. Sci. U.S.A.* **2000**, *97*, 1456–1460.

(11) Sinsa, S.; Anderson, J. P.; Barbour, R.; Basi, G. S.; Caccavello, R.; Davis, D.; Doan, M.; Dovey, H. F.; Frigon, N.; Hong, J.; Jacobson-Croak, K.; Jewett, N.; Keim, P.; Knops, J.; Lieberburg, I.; Power, M.; Tan, H.; Tatsuno, J.; Tung, J.; Schenk, D.; Seubert, P.; Suomensaari, S. M.; Wang, S.; Walker, D.; Zhao, J.; McColongue, L.; John, V. Purification and cloning of amyloid precursor protein β-secretase from human brain. *Nature* **1999**, *402*, 537–540.

(12) Vassar, R.; Bennett, B. D.; Babu-Khan, S.; Kahn, S.; Mendiaz, E. A.; Denis, P.; Teplow, D. B.; Ross, S.; Amarante, P.; Loeloff, R.; Luo, Y.; Fischer, S.; Fuller, J.; Edenson, S.; Lile, J.; Jarosinski, M. A.; Biere, A. L.; Curran, E.; Burgess, T.; Louis, J.-C.; Collins, F.; Treanor, J.; Rogers, G.; Citron, M. β-Secretase cleavage of Alzheimer's amyloid precursors protein by transmembrane aspartic protease BACE. *Science* **1999**, *286*, 735–741.

(13) Sinha, S.; Lieberburg, I. Cellular mechanisms of b-amyloid production and secretion. *Proc. Natl. Acad. Sci. U.S.A.* **1999**, *96*, 11049–11053.

(14) Selkoe, D. Toward a comprehensive theory for Alzheimer's disease. Hypothesis: Alzheimer's disease is caused by the cerebral accumulation and cytotoxicity of amyloid b-protein. *Ann. N.Y. Acad. Sci.* **2000**, *924*, 17–25.

(15) Coughlan, C.; Breen, K. C. Factors influencing the processing and function of the amyloid b precursor protein—a potential therapeutic target of Alzheimer's disease? *Pharmacol. Ther.* **2000**, *86*, 111–144.

(16) Racchi, M.; Govoni, S. Rationalizing a pharmacological intervention on the amyloid precursor protein metabolism. *Trends Pharmacol. Sci.* **1999**, *20*, 418–423.

(17) Jacobsen, S.; Reinhart, P.; Pangalos, M. Current concepts in therapeutic strategies targeting cognitive decline and disease modification in Alzheimer's disease. *Neurotherapeutics* **2005**, *2*, 612–626.

(18) Ghosh, A.; Kumaragurubaran, N.; Tang, J. Recent developments of structure-based β-secretase inhibitor's for Alzheimer's disease. *Curr. Top. Med. Chem.* **2005**, *5*, 1609–1622.

(19) Cumming, J. N.; Iserloh, U.; Kennedy, M. E. Design and development of BACE1 inhibitors. *Curr. Opin. Drug Discovery Dev.* **2004**, *7*, 536–556.

(20) Durham, T. B.; Shepherd, T. A. Progress toward the discovery and development of efficacious BACE inhibitors. *Curr. Opin. Drug Discovery Dev.* **2006**, *9*, 776–791.

(21) Baxter, E. W.; Reitz, A. B. BACE inhibitors for the treatment of Alzheimer's disease. *Annu. Rep. Med. Chem.* **2005**, *40*, 35–48.

(22) Schmidt, B.; Baumann, S.; Braub, H. A.; Larbig, G. Inhibitors and modulators of β- and γ-secretase. *Curr. Top. Med. Chem.* **2006**, *6*, 377–392.

(23) Guo, T.; Hobbs, D. W. Development of BACE1 inhibitors for Alzheimer's disease. *Curr. Med. Chem.* **2006**, *13*, 1811–1829.

(24) John, V.; Beck, J. P.; Bienkowski, M. J.; Sinha, S.; Heinrikson, R. Human β-secretase (BACE) and BACE inhibitors. *J. Med. Chem.* **2003**, *46*, 4625–4630.

(25) Carmen Villaverde, M.; Gonzalez-Louro, L.; Sussman, F. The search for drug leads targeted to the β-secretase: an example of the roles of computer assisted approaches in drug discovery. *Curr. Top. Med. Chem.* **2007**, *7*, 980–990.

(26) Hong, L.; Koelsch, Lin, X.; Wu, S.; Terzyan, S.; Ghosh, A.; Zhang, X. C.; Tang, J. Structure of the protease domain of memapsin 2(β-secretase) complexed with inhibitor. *Science* **2000**, *290*, 150–153.

(27) Stachel, S. J.; Coburn, C. A.; Steele, T. G.; Jones, K. G.; Loutzenhiser, E. F.; Gregro, A. R.; Rajapakse, H. A.; Lai, M.-T.; Crouthamel, M.-C.; Xu, M.; Tugusheva, K.; Lineberger, J. E.; Pietrak, B. L.; Espeseth, A. S.; Shi, X.-P.; Chen-Dodson, E.; Holloway, M. K.; Munshi, S.; Simon, A. J.; Kuo, L.; Vacca, J. P. Structure-based design of potent and selective cell-permeable inhibitors of human β-secretase (BACE1). *J. Med. Chem.* **2004**, *47*, 6447–6450.

(28) Coburn, C. A.; Stachel, S. J.; Li, Y.-M.; Rush, D. M.; Steele, T. G.; Chen-Dodson, E.; Holloway, M. K.; Xu, M.; Huang, Q.; Lai, M.-T.; DiMuzio, J.; Crouthamel, M.-C.; Shi, X.-P.; Sardana, V.; Chen, Z.; Munshi, S.; Kuo, L.; Makara, G. M.; Annis, D. A.; Tadikonda, P. K.; Nash, H. M.; Vacca, J. P. Identification of a small molecule nonpeptide active site β-secretase inhibitor that displays a nontraditional binding mode for aspartyl proteases. *J. Med. Chem.* **2004**, *47*, 6117–6119.

(29) Garino, C.; Pietrancosta, N.; Laras, Y.; Moret, V.; Rolland, A.; Quelever, G.; Kraus, J.-L. BACE1 inhibitory activities of new substituted phenyl-piperazine coupled to various heterocycles: chromene, coumarin, and quinoline. *Bioorg. Med. Chem. Lett.* **2006**, *16*, 1995–1999.

(30) Huang, D.; Luthi, U.; Kolb, P.; Cecchine, M.; Barberis, A.; Caflisch, A. In silico discovery of β-secretase inhibitors. *J. Am. Chem. Soc.* **2006**, *128*, 5436–5443.

(31) Huang, D.; Luethi, U.; Kolb, P.; Adler, K.; Cecchine, M.; Audedat, S.; Barberis, A.; Caflisch, A. A discovery of cell-permeable non-peptide inhibitors of b-secretase by high-throughput docking and continuum electrostatics calculations. *J. Med. Chem.* **2005**, *48*, 5108–5111.

(32) Rajapaske, H. A.; Nantermet, P. G.; Selnick, H. G.; Munshi, S.; McGaughey, G. B.; Lindsley, S. R.; Young, M. B.; Lai, M.-T.; Espeseth, A. S.; Shi, X.-P.; Colussi, D.; Pietrak, B.; Crouthamel, M.-C.; Tugusheva, K.; Huang, Q.; Simon, A. J.; Kuo, L.; Hazuda, D. J.; Graham, S.; Vacca, J. P. Discovery of oxadiazoyl tertiary carbinamine inhibitors of β-secretase (BACE1). *J. Med. Chem.* **2006**, *49*, 7270–7273.

(33) Edwards, P. D.; Albert, J. S.; Sylvester, M.; Aharony, D.; Andisik, D.; Callaghan, O.; Campbell, J. B.; Carr, R. A.; Chessari, G.; Congreve, M.; Frederickson, M.; Folmer, R. H.; Geschwindner, S.; Koether, G.; Kolmodin, K.; Krumrine, J.; Mauger, R. C.; Murray, C. W.; Olsson, L.; Patel, S.; Spear, N.; Tian, G. Application of fragment-based lead generation to the discovery of novel, cyclic amidine β-secretase inhibitors with manomolar potency, cellular activity and high ligand efficiency. *J. Med. Chem.* **2007**, *50*, 5912–5925.

(34) Murray, C, W.; Callaghan, O.; Chessari, A.; Congreve, M.; Frederickson, M.; Hartshorn, M. J.; McMenamin, R.; Patel, S.; Wallis, N. Application of fragment screening by X-ray crystallography to β-secretase. *J. Med. Chem.* **2007**, *50*, 1116–1123.

(35) Congreve, M.; Aharony, D.; Albert, J.; Callaghan, O.; Campbell, J.; Carr, R. A. E.; Chessari, G.; Cowan, S.; Edwards, P. D.; Frederickson, M.; McMenamin, R.; Murray, C. W.; Patel, S.; Wallis, N. Application of fragment screening by X-ray crystallography to the discovery of aminopyridines as inhibitors of β-secretase. *J. Med. Chem.* **2007**, *50*, 1124–1132.

(36) Geschwindner, S.; Olsson, L.-L.; Albert, J.; Deinum, J.; Edwards, P. D.; de Beer, T.; Folmer, R. H. A. Discovery of a novel warhead against β-secretase through fragment-based lead generation. *J. Med. Chem.* **2007**, *50*, 5903–5911.

(37) (a) Stanton, M.; Stauffer, S.; Gregro, A.; Steinbeiser, M.; Nantermet, P.; Sankaranarayanan, S.; Price, E.; Wu, G.; Crouthamel, M.-C.; Ellis, J.; Lai, M.-T.; Espeseth, A.; Shi, X.-P.; Jin, L.; Colussi, D.; Pietrak, B.; Huang, Q.; Xu, M.; Simon, A.; Graham, S.; Vacca, J.; Selnick, H. Discovery of isonicotinamide derived β-secretase inhibitors: in vivo reduction of β-amyloid. *J. Med. Chem.* **2007**, *50*, 3431–3433. (b) Baxter, E.; Conway, K.; Kennis, L.; Bischoff, F.; Mercken, M.; De Winter, H.; Reynolds, C.; Tounge, B.; Cuo, C.; Scott, M.; Huang, Y.; Braeken, M.; Pieters, S.; Berthelot, D.; Masure, S.; Bruinzeel, W.; Jordan, A.; Parker, M.; Boyd, R.; Qu, J.; Alexander, R.; Brenneman, D.; Reitz, A. 2-Amino-3,4-dihydroquinazolines as inhibitors of BACE-1 (β-site APP cleaving enzyme): use of structure based design to convert a micromolar hit into a nanomolar lead. *J. Med. Chem.* **2007**, *50*, 4261–4264. (c) Charrier, N.; Clarke, B.; Cutler, L.; Demont, E.; Dingwall, C.; Dunsdon, R.; East, P.; Hawkins, J.; Howes, C.; Hussain, I.; Jeffrey, P.; Maile, G.; Matico, R.; Mosley, J.; Naylor, A.; O'Brien, A.; Redshaw, S.; Rowland, P.; Soleil, V.; KSmith, K.; Sweitzer, S.; Theobald, P.; Vesey, D.; Walter, D.; Wayne, G. Second generation of hydroxyethylamine BACE-1 inhibitors: optimizing potency and oral bioavailability. *J. Med. Chem.* **2008**, *51*, 3313–3317. (d) Iserloh, U.; Wu, Y.; Cumming, J. N.; Pan, J.; Wang, L. Y.; Stamford, A. W.; Kennedy, M. E.; Kuvelkar, R.; Chen, X.; Parker, E. M.; Strickland, C.; Voigt, J. Potent pyrrolidine- and piperidine-based BACE-1 inhibitors. *Bioorg. Med. Chem. Lett.* **2008**, *18*, 414–417. (e) Iserloh, U.; Pan, J.; Stamford, A. W.; Kennedy, M. E.; Zhang, Q.; Zhang, L.; Parker, E. M.; Mchugh, N. A.; Favreau, L.; Strickland, C.; Voigt, J. Discovery of an orally efficaceous 4-phenoxypyrrolidine-based BACE-1 inhibitor. *Bioorg. Med. Chem. Lett.* **2008**, *18*, 418–422. (f) Clarke, B.; Demont, E.; Dingwall, C.; Dunsdon, R.; Faller, A.; Hawkins, J.; Hussain, I.; MacPherson, D.; Maile, G.; Matico, R.; Milner, P.; Mosley, J.; Naylor, A.; O'Brien, A.; Redshaw, S.; Riddell, D.; Rowland, P.; Soleil, V.; Smith, K.; SStanway, S. BACE-1 inhibitors part 2: identification of hydroxy ethylamines (HEAs) with reduced peptidic character. *Bioorg. Med. Chem. Lett.* **2008**, *18*, 1017–1021. (g) Beswick, P.; Charrier, N.; Clarke, B.; Demont, E.; Dingwall, C.; Dunsdon, R.; Faller, A.; Gleave, R.; Hawkins, J.; Hussain, I.; Johnson, C.; MacPherson, D.; Maile, G.; Matico, R.; Milner, P.; Mosley, J.; Naylor, A.; O'Brien, A.; Redshaw, S.; Riddell, D.; Rowland, P.; Skidmore, J.; VSoleil, V.; J. Smith, K.; Stanway, S.; Stemp, G.; Stuart, A.; Sweitzer, S.; Theobald, P.; Vesey, D.; Walter, D.; Ward, J.; Wayne, G. BACE-1 inhibitors part 3: identification of hydroxy ethylamines (HEAs) with nanomolar potency in cells. *Bioorg. Med. Chem. Lett.* **2008**, *18*, 1022–1026. (h) Park, H.; Min, K.; Kwak, H.-S.; Koo, K. D.; Lim, D.; Seo, S.-W.; Choi, J.-U.; Platt, B.; Choi., D.-Y. Synthesis, SAR, and X-ray structure of human BACE-1 inhibitors with cyclic urea derivatives. *Bioorg. Med. Chem. Lett.* **2008**, *18*, 2900–2904. (i) Cumming, J. N.; Le, T.; Babu, S.; Carroll, C.; Chen, X.; Favreau, L.; Gaspari, P.; Guo, T.; Hobbs, D.; Huang, Y.; Iserloh, U.; Kennedy, M.; Kuvelkar, R.; Li, G.; Lowrie, J.; McHugh, N.; Ozgur, L.; Pan, J.; Parker, E.; Saionz, K.; Stamford, A.; Strickland, C.; Tadesse, D.; Voigt, J.; Wang, L.; Wu, Y.; Zhang, L.; Zhang, Q. Rational design of novel, potent piperazinone and imidazolidinone BACE1 inhibitors. *Bioorg. Med. Chem. Lett.* **2008**, *18*, 3236–3241. (j) Charrier, N.; Clarke, B.; Cutler, L.; Demont, E.; Dingwall, C.; Dunsdon, R.; Hawkins, J.; Howes, C.; Hubbard, J.; Hussain, I.; Maile, G.; Matico, R.; Mosley, J.; Naylor, A.; O'Brien, A.; Redshaw, S.; Rowland, P.; Soleil, V.; Smith, K.; Sweitzer, S.; Theobald, P.; Vesey, D.; Walter, D.; Wayne, G. Second generation of BACE-1 inhibitors. Part 1: The need for improved pharmacokinetics. *Bioorg. Med. Chem. Lett.* **2009**, *19*, 3664–3668. (k) Redshaw, S.; Rowland, P.; Soleil, V.; Smith, K.; Sweitzer, S.; Theobald, P.; Vesey, D.; Walter, D.; Wayne, G. Second generation of BACE-1 inhibitors part 2: optimization of the non-prime side substituent. *Bioorg. Med. Chem. Lett.* **2009**, *19*, 3669–3673. (l) Charrier, N.; Clarke, B.; Cutler, L.; Demont, E.; Dingwall, C.; Dunsdon, R.; Hawkins, J.; Howes, C.; Hubbard, J.; Hussain, I.; Maile, G.; Matico, R.; Mosley, J.; Naylor, A.; O'Brien, A.; Redshaw, S.; Rowland, P.; Soleil, V.; Smith, K.; Sweitzer, S.; Theobald, P.; Vesey, D.; Walter, D.; Wayne, G. Second generation of BACE-1 inhibitors part 3: towards non hydroxyethylamine transition state mimetics. *Bioorg. Med. Chem. Lett.* **2009**, *19*, 3674–3678. (m) Barrow, J.; Rittle, K.; Ngo, P.; Selnick, H.; Graham, S.; Pitzenberger, S.; McGaughey, G.; Colussi, D.; Lai, M.-T.; Huang, Q.; Tugusheva, K.; Espeseth, A.; Simon, A.; Munshi, S.; Vacca, J. Design and synthesis of 2,3,5-substituted imidazolidin-4-one inhibitors of BACE-1. *ChemMedChem* **2007**, *2*, 995–999.

(38) Miyaura, N.; Suzuki, A. Palladium-catalyzed cross-coupling reactions of organoboron compounds. *Chem. Rev.* **1995**, *95*, 2457–2483.

(39) Stille, J. K. The palladium-catalyzed cross-coupling reactions of organotin reagents with organic electrophiles. *Angew. Chem., Int. Ed. Engl.* **1986**, *25*, 508–524.

(40) Wu, P.; Brand, L. Resonance energy transfer: methods and applications. *Anal. Biochem.* **1994**, *218*, 1–13.

(41) Malamas, M. S.; Erdei, J.; Gunawan, I.; Barnes, K.; Johnson, M.; Hui, Y.; Turner, J.; Hu, Y.; Wagner, E.; Fan, K.; Olland, A.; Bard, J.; Robichaud, A. Amino-imidazoles as Potent and selective human β-secretase (BACE1) inhibitors. *J. Med. Chem.* **2009**, *52*, 6314–6323.

(42) Hsiao, K.; Chapman, P.; Nilsen, S.; Eckman, C.; Harigaya, Y.; Younkin, S.; Yang, F.; Cole, G. Correlative memory deficits, Abeta elevation, and amyloid plaques in transgenic mice. *Science* **1996**, *274*, 99–102.

(43) Otwinowski, Z.; Minor, W. Processing of X-ray diffraction data collected in oscillation mode. *Methods Enzymol.* **1997**, *276*, 307–326.

(44) The CCP4 suite: programs for protein crystallography. *Acta Crystallogr., Sect. D: Biol. Crystallogr.* **1994**, *50* (Part 5), 760−763.

(45) Adams, P. D.; Grosse-Kunstleve, R. W.; Hung, L.-W.; Ioerger, T. R.; McCoy, A. J.; Moriarty, N. W.; Read, R. J.; Sacchettini, J. C.; Sauter, N. K.; Terwillinger, T. C. PHENIX: building new software for automated crystallographic structure determination. *Acta Crystallogr.* **2002**, *D58*, 1948–1954.

(46) Emsley, P.; Cowtan, K. Coot: model-building tools for molecular graphics. *Acta Crystallogr., Sect. D: Biol. Crystallogr.* **2004**, *60* (Part 12, No. 1), 2126–2132.

(47) McMartin, C.; Bohacek, R. S. *J. Computer-Aided Mol. Des.* **1997**, *11*, 333–344.